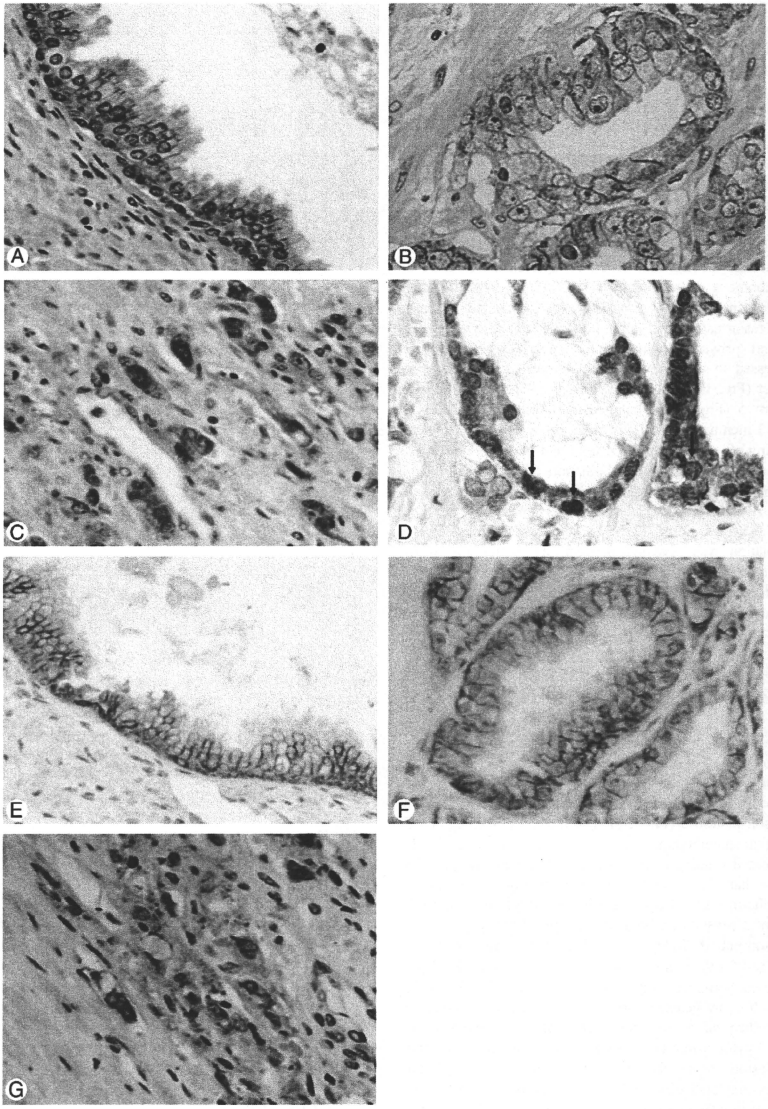
A
B
C
D
E
F
G

membranous expression, E-cadherin membranous expression, age, preoperative PSA concentration, Gleason score, pT stage, and surgical margin. P values less than .05 were considered statistically significant.

3. Results

3.1. NDRG1/Cap43 expression in the membrane, cytoplasm, and nucleus of prostate cancer cells in tumor tissue

NDRG1/Cap43 was predominantly expressed in the membrane of normal prostatic epithelium (Fig. 1A). Membranous expression of NDRG1/Cap43 was preserved in Gleason pattern 3 prostate cancer (Fig. 1B) and decreased in Gleason pattern 5 (Fig. 1C) compared to that in adjacent normal prostatic epithelium. NDRG1/Cap43 was not expressed in the cytoplasm in Gleason pattern 3 prostate cancer (Fig. 1B), but it was strongly expressed in Gleason pattern 5 (Fig. 1C). The median percentage of NDRG1/Cap43 membrane positive tumor cells was 60%. Decreased staining of membranous NDRG1/Cap43 was defined as less than 60% staining of the population of tumor cells. High cytoplasmic expression of NDRG1/Cap43 was defined as the intensity level 2 or 3. When individual tumors were analyzed for the expression of NDRG1/Cap43, a significant inverse correlation was revealed between its expression in the membrane and that in the cytoplasm ($r = -0.5033$; $P < .0001$, by Spearman rank correlation analysis; Fig. 2A). Furthermore, the nuclear expression of NDRG1/cap43 was observed in 11 cases (Fig. 1D).

3.2. Close association of NDRG1/Cap43 with E-cadherin expression

Expression of E-cadherin was predominantly expressed in the membrane of normal prostatic epithelium (Fig. 1E) and preserved in Gleason pattern 3 prostate cancer (Fig. 1F). Membranous expression of E-cadherin was decreased in Gleason pattern 5 (Fig. 1G). The median percentage of E-cadherin membranous positive tumor cells was 63.5%. Decreased staining of membranous E-cadherin was defined as less than 63.5% staining of the population of tumor cells. E-cadherin was not expressed in the cytoplasm in Gleason pattern 3 prostate cancer (Fig. 1F), but it was expressed in Gleason pattern 5 (Fig. 1G). When individual tumors were analyzed for the membranous expression of NDRG1/Cap43 and E-cadherin, a strong correlation was found ($r = 0.7130$; $P < .0001$, by Pearson correlation coefficient analysis; Fig. 2B). When individual tumors were analyzed for the NDRG1/Cap43 cytoplasmic expression and E-cadherin cytoplasmic expression, the number of patients with same cytoplasmic expression level was 25 (17%), 27 (18%), and 17 (11%) patients in intensity level 0, 1, and 2, respectively. NDRG1/

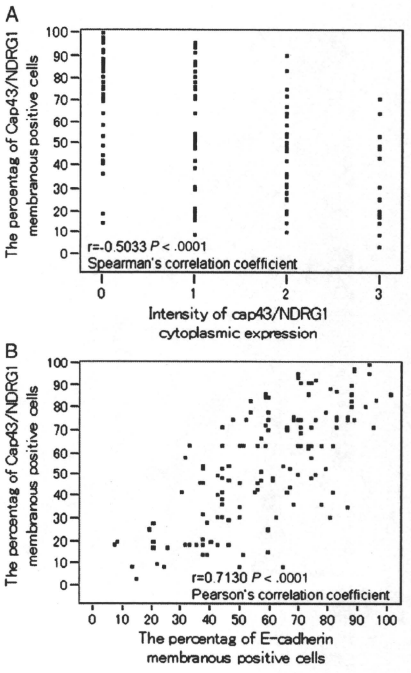

Fig. 2 (A) Inverted correlation was observed between the percentage of NDRG1/Cap43 membranous positive cells and the intensity of NDRG1/Cap43 cytoplasmic expression in tumor tissue ($r = -0.5033$; $P < .0001$, by Spearman rank correlation analysis). (B) There was significant correlation between NDRG1/Cap43 membranous expression and E-cadherin membranous expression in tumor tissue ($r = 0.7130$; $P < .0001$, by Pearson correlation coefficient analysis).

Cap43 cytoplasmic expression have a significant correlation with E-cadherin cytoplasmic expression ($r = 0.5847$; $P < .0001$, by Spearman rank correlation analysis).

3.3. Clinicopathologic parameters and disease-free survival analysis

In Table 2, we have summarized the correlations between NDRG1/Cap43 expression and clinicopathologic parameters. NDRG1/Cap43 membranous expression was significantly decreased in higher Gleason score compared to lower Gleason score cancer ($P \leq .0001$). Higher NDRG1/Cap43 cytoplasmic expression was associated with higher Gleason score ($P = .003$). NDRG1/Cap43 membranous expression

Table 2 Relationship between the expression of NDRG1/Caqp43 and various clinicopathologic characteristic

Variable	Membranous expression			*P*	Cytoplasmic expression		*P*
	n	Preserved	Decreased		Low	High	
Age							
<70	99	48	51	.4483	62	37	.8687
≥70	49	27	22		30	19	
PSA							
<10	89	49	40	.3094	56	33	.996
≥10	54	25	29		34	20	
Gleason score							
≤6	47	35	12	<.0001 [a]	38	9	.003 [b]
7	89	39	50		49	40	
≥8	12	1	11		5	7	
Stage							
pT2	101	56	45	.0882	65	36	.4214
pT3-4	47	19	28		27	20	
Surgical margin							
Negative	81	43	38	.5188	50	31	.9048
Positive	67	32	35		42	25	

[a] Statistically significant (Fisher extract test).
[b] Statistically significant (χ^2 test).

seemed to be decreased in pT3 or more advanced cancer, compared to pT2 cancer, but the difference was not statistically significant (P = .0882). Nuclear expression of NDRG1/Cap43 was not associated with preoperative PSA concentration (P = .5941), Gleason score (P = .9448), or stage (P = .7358).

Patients with decreased NDRG1/Cap43 membranous expression had lower disease-free survival rates, compared with the preserved expression group (log-rank test, P = .0002; Fig. 3A). The patients with high NDRG1/Cap43 cytoplasmic expression seemed to have lower disease-free survival rates than those of patients in the low expression group, but the difference was not statistically significant (log-rank test, P = .2584; Fig. 3B). Table 3 summarized the result of PSA recurrence-free survival analyzed by univariate and multivariate analysis. The Cox proportional hazards model revealed that decreased NDRG1/Cap43 membranous expression (P = .0175), high PSA level (P = .001), and higher Gleason score (P = .0455) were independent prognostic factors (Table 3). E-cadherin membranous expression was proved to be prognostic factor by univariate analysis (P = .0086); however, it could not be predictive independent prognostic factor by multivariate analysis (P = .9178; Table 3).

4. Discussion

To our knowledge, this is the first comprehensive immunohistochemical analysis to reveal the novel knowledge that the NDRG1/Cap43 expression in either the membrane or cytoplasm contributes to Gleason grade and

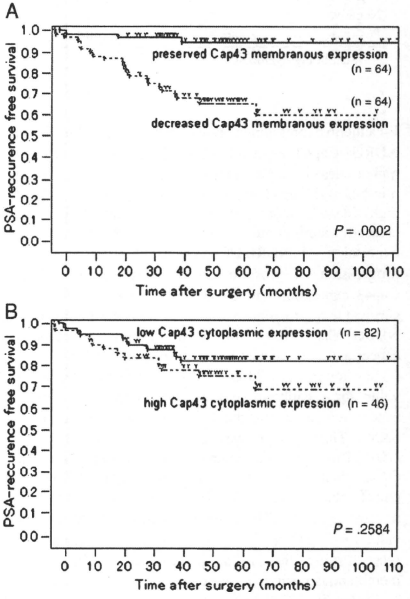

Fig. 3 Disease-free survival curves of patients in (A) NDRG1/Cap43 preserved and decreased membranous expression groups and (B) NDRG1/Cap43 low and high cytoplasmic expression groups.

Table 3 PSA recurrence-free survival in Cox regression analysis

	PSA recurrence-free survival univariate analysis		*P*	PSA recurrence-free survival multivariate analysis		*P*
	Hazard ratio	95%CI		Hazard ratio	95%CI	
Cap43/NDRG1 membranous expression						
Preserved	1			1		
Decreased	6.052	2.316-20.69	<.0001 [a]	4.008	1.263-15.37	.0175 [a]
E-cadherin membranous expression						
Preserved	1			1		
Decreased	2.981	1.308-7.638	.0086 [a]	1.058	0.367-3.230	.9178
Age						
<70	1			1		
≥70	1.191	0.522-2.588	.667	0.9384	0.380-2.182	.885
Preoperative PSA (ng/mL)						
<10.0	1			1		
≥10.0	4.645	2.084-11.33	.0001 [a]	4.185	1.769-10.73	.001 [a]
Gleason score						
≤6	1			1		
7	3.096	1.044-178.6		1.684	0.270-56.80	
≥8	13.13	14.30-3617	.0003 [a]	5.057	1.620-668.2	.0455 [a]
Pathologic stage						
pT2	1			1		
pT3-4	3.45	1.590-7.603	.002 [a]	1.462	0.571-3.816	.4289
Surgical margin						
Negative	1			1		
Positive	2.486	1.130-5.851	.0232 [a]	1.356	0.509-3.772	.5459

[a] Statistically significant.

E-cadherin expression in prostate cancer tissue. Membranous NDRG1/Cap43 expression was significantly decreased in higher Gleason score prostate cancer. By contrast, cytoplasmic NDRG1/Cap43 expression was significantly higher in high Gleason score prostate cancer, suggesting that decreased membranous expression and high cytoplasmic expression of NDRG1/Cap43 might be related to the progression of prostate cancer. Membranous NDRG1/Cap43 expression had a significant impact on disease-free survival in multivariate analysis. There is clear evidence that NDRG1/Cap43 has a role in the development of prostate cancer and may be useful as a prognostic marker.

Seventy percent [23,28] and 40% [29] were used as cutoff value for E-cadherin in the previous studies of prostate cancer. It is reasonable that the cutoff value for E-cadherin is 63.5%. Thirty percent was used as cutoff value for Cap43/NDRG1 in pancreatic cancer [16]. This number is lower than 60%, which is our cutoff value for Cap43/NDRG1. The cutoff value of Cap43/NDRG1 has been not clearly defined in prostate cancer. Therefore, the justification for the cutoff value for Cap43/NDRG1 remains unclear at present. In the present study, the median percentage of NDRG1/Cap43 membranous positive tumor cells was used as cutoff value.

Lachat et al [24] had previously reported that NDRG1/Cap43 expression is predominantly localized in the nucleus of prostate epithelium. However, others have reported that Cap43 is localized in both the cytoplasm and membrane [9,30]. In our study, NDRG1/Cap43 was localized predominantly in both the cytoplasm and membrane of normal epithelial cells and cancer cells. The nuclear expression of NDRG1/Cap43 was observed in only 11 cases, and nuclear NDRG1/Cap43 expression was found to be not associated with Gleason score, stage, or preoperative PSA concentration. Further analysis with more nuclear-positive samples will clarify the specific function of the nuclear localization of NDRG1/Cap43.

Bandyopadhyay et al [9] have reported that the NDRG1/Cap43 expression was significantly decreased in cases of higher Gleason score prostate cancer and also that NDRG1/Cap43 expression was correlated with the overall survival rate of patients. Furthermore, NDRG1/Cap43 inhibited lung colonization of metastatic prostate cancer cells, indicating that NDRG1/Cap43 is a metastasis suppressor gene [9]. Caruso et al [30] have demonstrated 3 different expression patterns for NDRG1/Cap43 in the membrane, cytoplasm, and nucleus in prostate cancer samples, but there was no conclusive NDRG1/Cap43 up-regulation or down-regulation in malignant progression in prostate cancer. On the other hand, our present study demonstrated that decreased membranous NDRG1/Cap43 expression is correlated with higher Gleason score and disease-free survival rates, and high cytoplasmic NDRG1/Cap43 expression is correlated with higher Gleason score. NDRG1/Cap43 membranous expression seemed to be decreased in pT3 or more advanced

cancer, compared to pT2 cancer. However, the difference was not statistically significant (P = .0882). The difference might be significant in further analysis with more samples. One might ask why NDRG1/Cap43 expression differentially affected progression states and survival in the studies by Bandyopadhyay et al [9], Caruso et al [30], and us. Although the reasons for this discrepancy remain unclear at present, the most likely places to search for the causes of critical differences will be how tumor specimens were obtained and how immunohistochemical expressions were analyzed. In the study by Bandyopadhyay et al [9], the prostate tissue specimens from patients were obtained from 3 different procedures, including needle biopsy, transurethral resection, and radical prostatectomy, whereas we evaluated the prognosis by using a cohort study in which radical prostatectomy was the only therapeutic procedure. Furthermore, Bandyopadhyay et al [9] did not elucidate whether the NDRG1/Cap43 expression was in the membrane or in the cytoplasm of the tumor cells, and Caruso et al [30] have demonstrated 3 different expression patterns, whereas we evaluated the membranous and the cytoplasmic expression, respectively and statistically.

Membrane labeling of NDRG1/Cap43 was observed predominantly adjacent to adherent junctions of colon tissue [24]. NDRG1/Cap43 has been observed to be involved in the expression of E-cadherin in a colon cancer [8], a lung cancer [25], and prostate cancer [26]. Furthermore, it was reported that staining of NDRG1/Cap43, which shuttled between cytoplasm and membrane, colocalized with staining of E-cadherin in prostate cancer cells by immunofluorescence analysis [26]. These findings are consistent with our data, describing that the membranous and the cytoplasmic expression patterns of NDRG1/Cap43 is very close to the expression patterns of E-cadherin. Cap43/NDRG1 might have a function of adherence in prostate. The decreased E-cadherin membranous expression has been reported to be a poor prognostic marker in prostate cancer [21,23]. In our study, univariate analysis revealed that the decreased E-cadherin membranous expression was poor prognostic factor; however, multivariate analysis failed to reveal that the decreased E-cadherin membranous expression was independent prognostic factor. In contrast, both univariate and multivariate analysis showed that the decreased NDRG1/Cap43 membranous expression was predictive poor prognostic factor. These results are suggesting that the decreased Cap43/NDRG1 membranous expression might be poorer prognostic marker in prostate, compared with decreased expression of E-cadherin. Furthermore, the relation between the membranous and the cytoplasmic expression of NDRG1/Cap43 was revealed to be significantly inverse. The results are indicating that a translocation of NDRG1/Cap43 might have an important role in the progression of prostate cancer via the regulation of E-cadherin.

In conclusion, our findings demonstrate that NDRG1/Cap43 may represent a novel marker of malignant progression and poor prognosis in prostate cancer. Furthermore, our data show that the NDRG1/Cap43 expression is involved with E-cadherin expression.

References

[1] Jemal A, Siegel R, Ward E, Murray T, Xu J, Thun MJ. Cancer statistics, 2007. CA Cancer J Clin 2007;57:43-66.

[2] Han M, Partin AW, Zahurak M, Piantadosi S, Epstein JI, Walsh PC. Biochemical (prostate specific antigen) recurrence probability following radical prostatectomy for clinically localized prostate cancer. J Urol 2003;169:517-23.

[3] Zhou D, Salnikow K, Costa M. Cap43, a novel gene specifically induced by Ni2+ compounds. Cancer Res 1998;58:2182-9.

[4] van Belzen N, Dinjens WN, Diesveld MP, et al. A novel gene which is up-regulated during colon epithelial cell differentiation and down-regulated in colorectal neoplasms. Lab Invest 1997;77:85-92.

[5] Taketomi Y, Sugiki T, Saito T, et al. Identification of NDRG1 as an early inducible gene during in vitro maturation of cultured mast cells. Biochem Biophys Res Commun 2003;306:339-46.

[6] Piquemal D, Joulia D, Balaguer P, Basset A, Marti J, Commes T. Differential expression of the RTP/Drg1/Ndr1 gene product in proliferating and growth arrested cells. Biochim Biophys Acta 1999;1450:364-73.

[7] Kurdistani SK, Arizti P, Reimer CL, Sugrue MM, Aaronson SA, Lee SW. Inhibition of tumor cell growth by RTP/rit42 and its responsiveness to p53 and DNA damage. Cancer Res 1998;58:4439-44.

[8] Guan RJ, Ford HL, Fu Y, Li Y, Shaw LM, Pardee AB. Drg-1 as a differentiation-related, putative metastatic suppressor gene in human colon cancer. Cancer Res 2000;60:749-55.

[9] Bandyopadhyay S, Pai SK, Gross SC, et al. The Drg-1 gene suppresses tumor metastasis in prostate cancer. Cancer Res 2003;63:1731-6.

[10] Bandyopadhyay S, Pai SK, Hirota S, et al. PTEN up-regulates the tumor metastasis suppressor gene Drg-1 in prostate and breast cancer. Cancer Res 2004;64:7655-60.

[11] Cangul H. Hypoxia upregulates the expression of the NDRG1 gene leading to its overexpression in various human cancers. BMC Genet 2004;5:27.

[12] Cangul H, Salnikow K, Yee H, Zagzag D, Commes T, Costa M. Enhanced expression of a novel protein in human cancer cells: a potential aid to cancer diagnosis. Cell Biol Toxicol 2002;18:87-96.

[13] Chen J, Li S, Yang Z, Lu G, Hu H. Correlation between NDRG1 and PTEN expression in endometrial carcinoma. Cancer Sci 2008;99:706-10.

[14] Wang Z, Wang F, Wang WQ, et al. Correlation of N-*myc* downstream-regulated gene 1 overexpression with progressive growth of colorectal neoplasm. World J Gastroenterol 2004;10:550-4.

[15] Chua MS, Sun H, Cheung ST, et al. Overexpression of NDRG1 is an indicator of poor prognosis in hepatocellular carcinoma. Mod Pathol 2007;20:76-83.

[16] Maruyama Y, Ono M, Kawahara A, et al. Tumor growth suppression in pancreatic cancer by a putative metastasis suppressor gene Cap43/NDRG1/Drg-1 through modulation of angiogenesis. Cancer Res 2006;66:6233-42.

[17] Angst E, Sibold S, Tiffon C, et al. Cellular differentiation determines the expression of the hypoxia-inducible protein NDRG1 in pancreatic cancer. Br J Cancer 2006;95:307-13.

[18] Fotovati A, Fujii T, Yamaguchi M, et al. 17Beta-estradiol induces down-regulation of Cap43/NDRG1/Drg-1, a putative differentiation-related and metastasis suppressor gene, in human breast cancer cells. Clin Cancer Res 2006;12:3010-8.

[19] Koshiji M, Kumamoto K, Morimura K, et al. Correlation of N-*myc* downstream-regulated gene 1 expression with clinical outcomes of colorectal cancer patients of different race/ethnicity. World J Gastroenterol 2007;13:2803-10.

[20] Nishio S, Ushijima K, Tsuda N, et al. Cap43/NDRG1/Drg-1 is a molecular target for angiogenesis and a prognostic indicator in cervical adenocarcinoma. Cancer Lett 2008;264:36-43.
[21] Umbas R, Isaacs WB, Bringuier PP, et al. Decreased E-cadherin expression is associated with poor prognosis in patients with prostate cancer. Cancer Res 1994;54:3929-33.
[22] Morton RA, Ewing CM, Nagafuchi A, Tsukita S, Isaacs WB. Reduction of E-cadherin levels and deletion of the alpha-catenin gene in human prostate cancer cells. Cancer Res 1993;53:3585-90.
[23] De Marzo AM, Knudsen B, Chan-Tack K, Epstein JI. E-cadherin expression as a marker of tumor aggressiveness in routinely processed radical prostatectomy specimens. Urology 1999;53:707-13.
[24] Lachat P, Shaw P, Gebhard S, van Belzen N, Chaubert P, Bosman FT. Expression of NDRG1, a differentiation-related gene, in human tissues. Histochem Cell Biol 2002;118:399-408.
[25] Stein S, Thomas EK, Herzog B, et al. NDRG1 is necessary for p53-dependent apoptosis. J Biol Chem 2004;279:48930-40.
[26] Kachhap SK, Faith D, Qian DZ, et al. The N-*myc* down regulated Gene1 (NDRG1) Is a Rab4a effector involved in vesicular recycling of E-cadherin. PLoS ONE 2007;2:e844.
[27] Koksal IT, Ozcan F, Kilicaslan I, Tefekli A. Expression of E-cadherin in prostate cancer in formalin-fixed, paraffin-embedded tissues: correlation with pathological features. Pathology 2002;34: 233-8.
[28] Rubin MA, Mucci NR, Figurski J, Fecko A, Pienta KJ, Day ML. E-cadherin expression in prostate cancer: a broad survey using high-density tissue microarray technology. athol 2001;32:690-7.
[29] Kuczyk M, Serth J, Machtens S, et al. Expression of E-cadherin in primary prostate cancer: correlation with clinical features. Br J Urol 1998;81:406-12.
[30] Caruso RP, Levinson B, Melamed J, et al. Altered N-*myc* downstream-regulated gene 1 protein expression in African-American compared with Caucasian prostate cancer patients. Clin Cancer Res 2004;10 (1 Pt 1):222-7.

Inhibition of translation by cytotrienin A—a member of the ansamycin family

LISA LINDQVIST,[1] FRANCIS ROBERT,[1] WILLIAM MERRICK,[2] HIDEAKI KAKEYA,[3] CHRISTOPHER FRASER,[4] HIROYUKI OSADA,[5] and JERRY PELLETIER[1,6]

[1]Department of Biochemistry, McGill University, Montreal, Quebec H3G 1Y6, Canada
[2]Department of Biochemistry, School of Medicine, Case Western Reserve University, Cleveland, Ohio 44106, USA
[3]Department of System Chemotherapy and Molecular Sciences, Graduate School of Pharmaceutical Sciences, Kyoto University, Kyoto 606-8501, Japan
[4]Department of Molecular and Cellular Biology, UC Davis, University of California, Davis, California 95616, USA
[5]Chemical Biology Department, Advanced Science Institute, RIKEN, Wako-shi, Saitama 351-0198, Japan
[6]The Rosalind and Morris Goodman Cancer Centre, McGill University, Montreal, Quebec H3G 1Y6, Canada

ABSTRACT

The ansamycins are a diverse and often physiologically active group of compounds that include geldanamycin and rifamycin, inhibitors of heat shock protein 90 and prokaryotic DNA-dependent RNA synthesis, respectively. Cytotrienin A is an ansamycin-type small molecule with potent antiproliferative and proapoptotic properties. Here, we report that this compound inhibits eukaryotic protein synthesis by targeting translation elongation and interfering with eukaryotic elongation factor 1A function. We also find that cytotrienin A prevents HUVEC tube formation and diminishes microvessel formation in the chorioallantoic membrane assay. These results provide a molecular understanding into cytotrienin A's previously reported properties as an anticancer apoptosis-inducing drug.

Keywords: cytotrienin A; eEF1A; translation inhibitor; protein synthesis

INTRODUCTION

There is much interest in identifying and characterizing novel inhibitors of eukaryotic protein synthesis, both as tools to characterize the translation machinery and as drugs that can curtail malignant cell proliferation (Pelletier and Peltz 2007). There are several observations that suggest a high therapeutic index can be achieved by inhibiting translation in cancers. One vulnerability of cancer cells is at the level of ribosome recruitment, where mRNAs must compete with each other for limiting amounts of translation initiation factors (Duncan et al. 1987). Translation of mRNAs that are "weak" competitors for eukaryotic initiation factors (eIFs) are therefore more sensitive to small changes in the levels of these factors. Since several of the "weak" mRNAs characterized to date encode for antiapoptotic or prosurvival factors, their selective down-regulation preferentially curtails growth of tumor cells in preclinical cancer models (Graff et al. 2007; Cencic et al. 2009; Lucas et al. 2009). In addition, translation initiation inhibitors have been shown to exert antiangiogenic activities, a property that may contribute to their anti-cancer activity (Graff et al. 2007; Cencic et al. 2009). Additionally, the rapid reduction in levels of pro-oncogenic and pro-survival proteins having short half-lives (Chao et al. 1998; Nijhawan et al. 2003) occurs upon translation inhibition, and this can impair the growth of transformed cells. Higher translation rates also occur in human tumors and appear to be required to maintain their oncogenic state (Heys et al. 1991; Wendel et al. 2004). These latter two points may explain why some inhibitors of translation elongation show efficacy in preclinical cancer models as well as in the clinic (Quintas-Cardama et al. 2009; Robert et al. 2009).

The first step of translation elongation is catalyzed by eukaryotic elongation factor (eEF) 1A, which delivers the aminoacyl-tRNA (aa-tRNA) to the ribosomal A site, followed by GTP hydrolysis (provided that the proper codon–anticodon interaction occurs). There are two isoforms of eEF1A, eEF1A1 and eEF1A2, which are encoded by separate genes and show 95% identity. Both isoforms are thought to

Reprint requests to: Jerry Pelletier, McIntyre Medical Sciences Building, Room 810, 3655 Promenade Sir William Osler, McGill University, Montreal, Quebec H3G 1Y6, Canada; e-mail: jerry.pelletier@mcgill.ca; fax: (514) 398-7384.

Article published online ahead of print. Article and publication date are at http://www.rnajournal.org/cgi/doi/10.1261/rna.2307710.

be functionally redundant for translation, although they are differentially expressed (Kahns et al. 1998) and both have been shown capable of acting as oncogenes in the appropriate setting (Thornton et al. 2003).

Here, we describe the characterization of a novel modulator of eEF1A from the ansamycin family. Cytotrienin A (Cyt A) is a natural product produced by *Streptomyces* sp., which has been previously reported to induce apoptosis in leukemia cell lines by activating c-Jun N-terminal kinase (JNK), p38 mitogen-activated protein kinase (MAPK), and p36 myelin basic protein (MBP) kinase (Kakeya et al. 1998; Watabe et al. 2000). Here, we report that Cyt A inhibits translation elongation by interfering with eEF1A function. Our results provide molecular insight into Cyt A's previously reported properties as an anti-cancer compound.

RESULTS

Cytotrienin A inhibits translation elongation

During the course of a high-throughput screen to identify translation inhibitors (Novac et al. 2004), Cyt A (Fig. 1A) was identified as a "hit" that inhibited both cap-dependent (Firefly [FF] luciferase) and hepatitis C virus (HCV)-driven (*Renilla* [Ren] luciferase) translation in Krebs-2 extracts

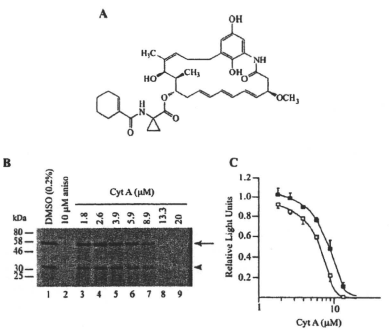

FIGURE 1. Cyt A inhibits eukaryotic translation. (*A*) Chemical structure of Cyt A. (*B*) Cyt A inhibits both cap-dependent and HCV IRES-driven translation in Krebs-2 extracts. In vitro translations were performed in the presence of [^{35}S]methionine and programmed with FF/HCV/Ren. DMSO, anisomycin (aniso), or Cyt A (lanes 3–9) were added to Krebs-2 extracts at the indicated concentrations. Proteins were separated by SDS-PAGE and visualized by autoradiography. The arrow and arrowhead denote Firefly and *Renilla* luciferase, respectively. (*C*) Luciferase activity from translations performed in Krebs-2 extracts programmed with FF/HCV/Ren shown in *B*. Light units were set relative to the values obtained in the presence of vehicle (DMSO). The average of three measurements is shown with the SEM represented by error bars.

(Fig. 1B,C) and in rabbit reticulocyte lysate (RRL) (data not shown). Cyt A was also active in wheat-germ extracts, but did not significantly inhibit prokaryotic translation in *E. coli* S30 extracts at 50 μM (data not shown). These results indicate that Cyt A inhibits both cap-dependent and IRES-dependent translation. To determine whether the initiation phase of translation was affected by Cyt A, we performed ribosome binding experiments to assess the effects of Cyt A on 80S complex formation (Fig. 2A). Cyt A was able to stabilize 80S complexes to a similar degree as cycloheximide (CHX) (Fig. 2A, left and right panels, respectively). As well, addition of the initiation inhibitor hippuristanol, followed by addition of Cyt A to the binding reactions, caused a decrease in 80S complex formation (Fig. 2A, left), similar to if Hipp alone was present in the binding reactions (Fig. 2A, right). However, if Cyt A was present in the extract prior to the addition of Hipp, 80S complexes were trapped to the same efficiency as observed for Cyt A (Fig. 2A, left). Consistent with these results, Cyt A inhibited the translation of poly(Phe) from poly(U) RNA (Fig. 2B). Taken together, these experiments strongly suggest that Cyt A targets translation elongation.

The elongation inhibitors homoharringtonine (HHT) and bruceantin (Bru) inhibit only newly initiated ribosomes during the first step of elongation and allow translating ribosomes to run-off mRNA templates (Pelletier and Peltz 2007; Robert et al. 2009). To determine whether Cyt A showed similar properties, we performed in vitro translation reactions in the presence of [^{35}S]methionine, where compound was added 5 min after the start of translation (Fig. 2C). A kinetic analysis was performed to quantitate the amount of product synthesized. Inhibition of translation by HHT is delayed by several minutes following its addition to a translating extract as polysomes run-off mRNA templates due to the reduced affinity of HHT for actively translating ribosomes (Fig. 2C; Chan et al. 2004). Addition of Cyt A immediately inhibited protein synthesis in a manner similar to CHX. These results indicate that Cyt A affects translating ribosomes and does not allow polysome run-off.

Cyt A modulates eEF1A-dependent aa-tRNA binding to the ribosome

To better understand the mechanism by which Cyt A inhibits elongation, we analyzed its effects on tRNA binding to the ribosome, peptide bond formation, and translocation. We first tested whether Cyt A could inhibit the peptidyl transferase activity of the ribosome by monitoring the formation of [^{35}S]methionyl-puromycin. Cyt A did not inhibit peptidyl transferase activity under these conditions, unlike the known peptdyl transferase inhibitor HHT (Fig. 3A).

We next assessed whether Cyt A could affect binding of aa-tRNA to ribosomes in eEF1A-independent [high poly(U)

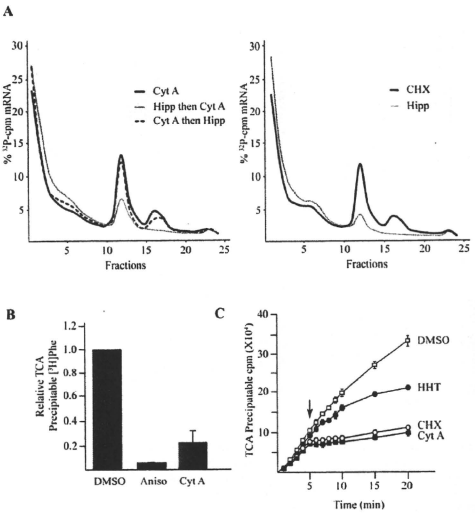

FIGURE 2. Cyt A inhibits translation elongation. (*A*) Cyt A does not inhibit translation initiation. Ribosome bindings were performed in RRL using ^{32}P-labeled CAT RNA. Reactions were separated by centrifugation on 10%–30% glycerol gradients and fractions quantitated by scintillation counting. (*Left*) Ribosome bindings were performed in the presence of 50 μM Cyt A alone, preincubated with 50 μM hippuristanol (Hipp), followed by addition of 50 μM Cyt A, or preincubated with 50 μM Cyt A, followed by the addition of 50 μM Hipp. (*Right*) Ribosome bindings were performed in the presence of 0.6 mM CHX or 50 μM Hipp. Both panels are part of the same experiment, but were separated for clarity. (*B*) Cyt A inhibits translation elongation. In vitro translations in RRL supplemented with [^{3}H]phenylalanine and programmed with poly(U) RNA. Polypeptides were TCA precipitated and quantitated by scintillation counting. Counts were set relative to DMSO levels. The average of four measurements is shown with the SEM. (*C*) Cyt A does not permit ribosome run-off. In vitro translation reactions of Krebs-2 extracts were allowed to proceed in the absence of compound for 5 min, after which time DMSO, HHT (200 μM), CHX (50 μM), or Cyt A (20 μM) were added. Aliquots were taken at the indicated times, TCA precipitated, and quantitated by scintillation counting. The average of three measurements is shown with the SEM. The downward arrow indicates the point of addition of compound or vehicle.

RNA concentration] or eEF1A-dependent [low poly(U) RNA concentration] reconstituted systems. The ability of [^{14}C]Phe-tRNA^{Phe} to bind ribosomes was not affected by Cyt A when binding was eEF1A independent (Fig. 3B), indicating that Cyt A does not compete with [^{14}C]Phe-tRNA^{Phe} for the ribosome. Under eEF1A-dependent conditions, the levels of ribosome-bound [^{14}C]Phe-tRNA^{Phe} in the presence of GDP or GMPPNP were similar to those binding reactions lacking eEF1A in DMSO controls (Fig. 3C). [Also note that tRNA binding without eEF1A in this experiment is much lower than in the experiment presented in Fig. 3B, due to a 1000-fold decrease in poly(U) RNA template.] In the presence of GTP, the amount of [^{14}C]Phe-tRNA^{Phe} bound to ribosomes increased significantly (Fig. 3C). Under this condition, both Cyt A and CHX decreased [^{14}C]Phe-tRNA^{Phe} binding by ~40%, while Did B had no significant effect. The low amount of [^{14}C]Phe-tRNA^{Phe} binding to ribosomes observed in the presence of GMPPNP was increased when either Cyt A or Did B was present in the reactions (Fig. 3C). One interpretation of this result is that Cyt A stabilizes the ternary complex on the ribosome (see Discussion).

eEF2-dependent translocation is inhibited by Cyt A only when aa-tRNA is delivered in an eEF1A-dependent manner

The ability of Cyt A to affect eEF2-dependent translocation was also investigated. After either nonenzymatic (as in Fig. 3B) or eEF1A-dependent aa-tRNA binding to the ribosome (with GTP, as in Fig. 3C), translocation was initiated by the addition of puromycin and eEF2. Under these conditions, CHX inhibited translocation regardless of whether [^{14}C]Phe-tRNA^{Phe} binding was eEF1A dependent or eEF1A independent, whereas Cyt A inhibited translocation only when charged tRNA was loaded in an eEF1A-dependent manner (Fig. 3D). Did B served as a positive control in the eEF1A-dependent translocation assay and was found to inhibit this reaction (Fig. 3D).

Cyt A inhibits neither ternary complex formation nor the GTPase activity of eEF1A

The inhibitory effect in the presence of GTP and stimulatory effect in the presence of GMPPNP of Cyt A on tRNA binding could result from improper ternary complex formation (eEF1A:GTP:aa-tRNA). To determine whether Cyt A affects the ability of eEF1A to bind to GTP, we performed a UV cross-linking experiment with [α-^{32}P]GTP in the presence or absence of Phe-tRNA^{Phe} (Fig. 4A). We observed no significant change in the efficiency of GTP cross-linking to eEF1A in the presence of Cyt A (Fig. 4A, cf. lanes 2 and 5 with 1 and 4, respectively). Excess GTP competed for the radiolabeled [α-^{32}P]GTP in this assay (cf. lane 3 and 6 with 1 and 4, respectively). As well, Cyt A did not prevent eEF1A:[^{14}C]-Phe-tRNA^{Phe} complex formation, as assessed by electrophoretic mobility shift assay (EMSA) (Fig. 4B). We investigated

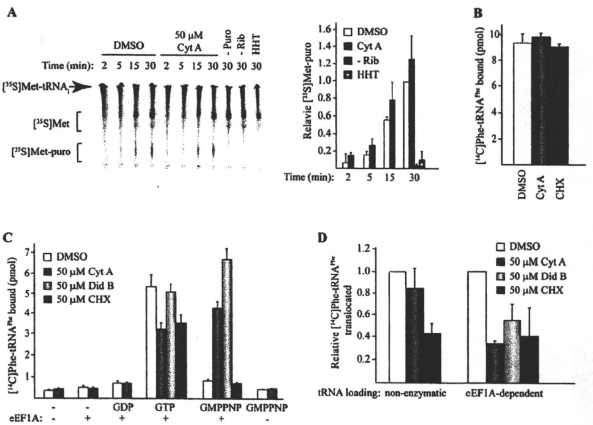

FIGURE 3. The effect of Cyt A on the steps of translation elongation. (*A*) Cyt A does not inhibit peptidyl transferase activity. [^{35}S]Methionine-puromycin formation was monitored in the presence of purified 40S and 60S ribosomes using [^{35}S]Met-tRNA$_i$ and ribosomal high-salt wash from RRL. (*Left*) Aliquots of samples were taken at the indicated time points and separated by TLC. The position of migration of [^{35}S]Met-puro, [^{35}S]Met, and [^{35}S]Met-tRNA$_i$ is indicated to the *left*. The addition of 50 μM Cyt A, 40 μM HHT, or the absence of puromycin (−Puro) or ribosomes (−Rib) is indicated at *top*. (*Right*) Quantitation of [^{35}S]Met-puro production. The average of four experiments relative to the DMSO control at 30 min is shown. Note that values obtained from the reaction in the absence of puromycin were subtracted as background. The SEM is represented using error bars. (*B*) Cyt A does not inhibit eEF1A-independent [^{14}C]Phe-tRNA^{Phe} binding to 80S ribosomes. Filter binding of [^{14}C]Phe-tRNA^{Phe} was performed with purified 80S ribosomes, 0.4 mg/mL poly(U) RNA, and either DMSO, 50 μM Cyt A, or 50 μM CHX. The average of four experiments is shown with the SEM indicated by error bars. (*C*) Cyt A modulates eEF1A-dependent [^{14}C]Phe-tRNA^{Phe} binding to 80S ribosomes. Filter binding of [^{14}C]Phe-tRNA^{Phe} with purified 80S ribosomes, and 0.4 μg/mL poly(U) RNA in the presence of either DMSO, 50 μM Cyt A, 50 μM DidB, or 50 μM CHX. The presence of eEF1A and nucleotide is indicated. The average of three to six measurements is shown with SEM indicated by error bars. (*D*) eEF2-dependent translocation of [^{14}C]Phe-tRNA^{Phe} is inhibited by Cyt A only when aminoacyl-tRNA is loaded in an eEF1A-dependent manner. Following nonenzymatic or eEF1A-dependent tRNA binding (as described in *B* and *C* with GTP, respectively), eEF2 was added to the reaction with puromycin. The amount of puromycin-active [^{14}C]Phe-tRNA^{Phe} was extracted with ethyl aceteate and quantitated by scintillation counting. tRNA already bound to the P-site was subtracted from these values (see Materials and Methods) and set relative to the DMSO control. The average of two to four experiments is shown with the SD.

whether Cyt A affects the GTPase activity of eEF1A and found no evidence to this effect (Fig. 4C). We conclude that Cyt A does not interfere with ternary complex formation.

Cellular protein synthesis is inhibited by Cyt A

[^{35}S]Methionine/cysteine labeling of HeLa cells was inhibited by Cyt A, whereas DNA and RNA synthesis was not dramatically affected (Fig. 5A). Inhibition of translation was reversible and showed almost complete recovery by 6 h after removal of the compound (Fig. 5B). The polysome profile of cells exposed to Cyt A for 1 h showed a similar to slight increase in polysomes compared with those isolated from cells exposed to vehicle (DMSO) (Fig. 5C). When hippuristanol was added during the last 30 min of Cyt A treatment, polysomes were still present, unlike what was observed when cells were exposed to only hippuristanol (Fig. 5C, left). Cells treated with HHT, which is known to allow ribosome run-off, showed an absence of polysomes (Fig. 5C, right). This data is consistent with Cyt A causing stalling of translating ribosomes and allowing their accumulation on mRNA templates.

Antiangiogenic properties of Cyt A

Inhibition of translation has been shown to impair angiogenesis and has been suggested as a mechanism by which they function as anti-cancer therapeutics (Taraboletti et al. 2004; Graff et al. 2007; Cencic et al. 2009). We therefore tested whether Cyt A might have similar properties. To examine this, we utilized a HUVEC tube formation assay, which has been previously used to mimic some aspects of angiogenesis (Kubota et al. 1988; Graff et al. 2007; Cencic et al. 2009). The inhibition of tube formation with Cyt A was dose dependent (Fig. 6A,B) at concentrations where

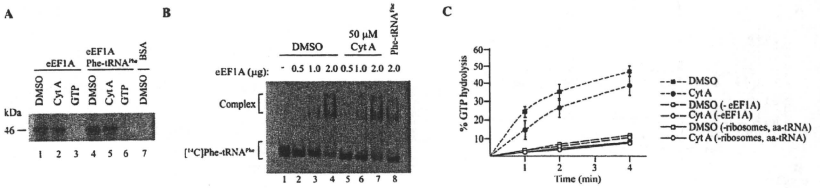

FIGURE 4. Cyt A does not affect ternary formation. (*A*) Cyt A does not inhibit GTP binding to eEF1A. Purified eEF1A (1 μg) was UV cross-linked to [α^{32}P]GTP in the presence (lanes *4–7*) or absence (lanes *1–3*) of Phe-tRNA^{Phe} and 50 μM Cyt A or 1 mM unlabeled GTP. Reactions were treated with RNase A, separated by SDS-PAGE, and visualized by autoradiography. (*B*) Cyt A does not affect [^{14}C]Phe-tRNA^{Phe} binding to eEF1A. Increasing amounts of eEF1A were incubated with [^{14}C]Phe-tRNA^{Phe} in the presence of DMSO, 50 μM Cyt A, or unlabeled Phe-tRNA^{Phe} competitor. EMSAs were performed on 6% polyacrylamide gels and visualized by autoradiography. The position of migration of free [^{14}C]Phe-tRNA^{Phe} and complexes are indicated to the *left*. (*C*) Cyt A does not affect the GTPase activity of eEF1A. eEF1A and [γ-^{32}P]GTP were incubated with 40S and 60S ribosomes and Phe-tRNA^{Phe} in the presence of 50 μM Cyt A or DMSO. GTPase activity was also measured in the absence of eEF1A or without ribosomes or Phe-tRNA^{Phe}. The average of three to four measurements is shown with the SEM represented as error bars.

general translation was inhibited by >90%, (Fig. 6C, open circles) similar to effects observed with silvestrol (Silv), a previously reported translation initiation inhibitor with antiangiogenic properties (Fig. 6A; data not shown) (Cencic et al. 2009). Importantly, cells remained viable under these conditions (Fig. 6C, squares). We also tested the ability of Cyt A to inhibit angiogenesis in the more physiological chorioallantoic membrane (CAM) assay. Cyt A inhibited new vessel growth in a dose-dependent manner (Fig. 6D), similar to the inhibitor of VEGF receptor tyrosine kinase Semaxanib (SU5416) (Riboldi et al. 2005).

DISCUSSION

Ansamycins form a diverse family of compounds exerting a number of physiological effects on mammalian and viral systems (Isaacs et al. 2003; Floss and Yu 2005). In this study, we identified a member of this family as an inhibitor of eukaryotic translation elongation. Other ansamycins such as rifabutin and 17-AAG did not inhibit protein synthesis in vitro in Krebs-2 extracts at 50 μM (data not shown), indicating that this is not a general property of this group of compounds.

Increasing evidence links deregulated protein synthesis and cancer growth (Lindqvist and Pelletier 2009). Indeed, two inhibitors of elongation (HHT and a derivative of Did B) have advanced to clinical trials (Le Tourneau et al. 2007; Quintas-Cardama et al. 2007). In addition, we have previously shown that inhibitors of elongation can sensitize select tumors to the pro-apoptotic properties of the clinical agent doxorubicin (Robert et al. 2009). Inhibition of translation could, in principle, suppress drug resistance by curtailing the synthesis of antiapoptotic proteins and/or drug transporters. Leukemic cell lines have been previously shown to be more sensitive to Cyt A-induced apoptosis compared with other tumor cell lines, supporting a potential therapeutic use of Cyt A in blood cancer treatment (Watabe et al. 2000). Here, we show that Cyt A inhibits protein synthesis in cell lines that were previously shown to be resistant to Cyt A-induced apoptosis (Fig. 5A) as well as in nontransformed HUVECs (Fig. 6C). Indeed HeLa, HUVEC, and Jurkat (a leukemia cell line previously shown to undergo apoptosis after a 24-h exposure to Cyt A [IC_{50} = 13.87 nM]; Watabe et al. 2000) cells all had very similar IC_{50}s with respect to translation inhibition (data not shown). These results suggest that the differential sensitivity of different cell lines to the apoptotic response is not due to a difference in sensitivity to Cyt A-induced protein synthesis inhibition but may depend on intrinsic factors that link the apoptotic response to the translation apparatus. We demonstrate that translation inhibition occurs well before apoptosis can be detected and, therefore, must precede the apoptotic response (Fig. 6C). The fact that Cyt A induces apoptosis more readily in leukemia is consistent with reports that B-cell and leukemia-cell lines also are more sensitive to the translation initiation inhibitor silvestrol compared with other cell types (Monks et al. 1991; Lucas et al. 2009).

Translation elongation can be inhibited in an eEF1A-dependent manner also by interfering with ternary complex formation (eEF1A:GTP:aminoacyl-tRNA). Indeed, several antibiotics target this step, including GE2770A and pulvomycin (Heffron and Jurnak 2000; Andersen et al. 2003). This mechanism is in contrast to that of Cyt A (Fig. 4A,B). Pulvomycin is known to increase the GTPase activity of EF-Tu, the bacterial homolog of eEF1A (Andersen et al. 2003), while both Did B and Cyt A do not alter GTPase activity of eEF1A to any significant extent (Fig. 4C; Crews et al. 1994; Ahuja et al. 2000). Therefore, the mechanism of action of Cyt A does not seem to be reminiscent of these EF-Tu-targeting inhibitors.

Cyt A stalled polyribosomes on mRNA templates and inhibited translating ribosomes, similar to what has been reported for the translation elongation inhibitors CHX and

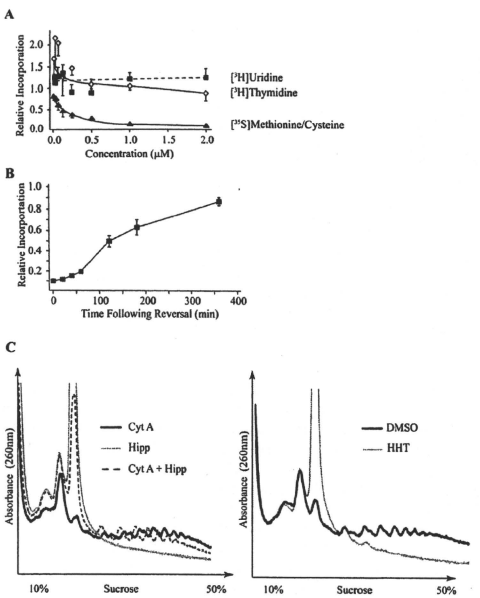

FIGURE 5. Cyt A reversibly inhibits translation in cell culture. (*A*) Consequences of Cyt A exposure on DNA, RNA, and protein synthesis in HeLa cells. Cyt A was added to cell medium for 1 h and [6-^{3}H]thymidine, [5-^{3}H]uridine, or [^{35}S]methionine/cysteine was present during the last 20 min of incubation. Counts from TCA-precipitated material were normalized to total protein content and set relative to the DMSO control. The average of four data points is shown with the SEM indicated by error bars. (*B*) Inhibition of translation by Cyt A is reversible. HeLa cells were incubated in 2 μM Cyt A for 1 h, after which fresh medium lacking Cyt A was added. Twenty minutes before lysis, [^{35}S]methionine/cysteine was added. Normalization was performed to total protein concentration and set relative to the DMSO control. The average of four measurements is shown with the SEM represented by error bars. (*C*) Cyt A does not allow ribosome run-off in cell culture. Polysome formation in HeLa cells exposed to 2 μM Cyt A for 1 h and/or 5 μM Hipp for 30 min or 0.5 μM HHT for 1 h. Panels are from the same experiment and were separated for clarity.

Did B (Fig. 5C; Urdiales et al. 1996; Schneider-Poetsch et al. 2010). In the eEF1A-dependent aa-tRNA-binding experiment (Fig. 3C), the amount of [^{14}C]Phe-tRNA^{Phe} bound to ribosomes was significantly reduced in the presence of GMPPNP compared with GTP (Fig. 3C). We believe this may be due to the large dilution (~100-fold) that occurs during processing of the samples for filter binding, allowing dissociation of the ternary complex from the ribosome. This is consistent with the finding that only after GTP hydrolysis is the charged tRNA locked in the A site (Rodnina and Wintermeyer 2001). Hence, one interpretation of our results is that in the presence of GMPPNP, the aa-tRNA is lost from the ribosome. However, this is not observed if Did B or Cyt A are present (Fig. 3C), suggesting that these compounds stabilize the aa-tRNA:ribosome interaction, perhaps by blocking release of eEF1A. Both Cyt A and Did B inhibited translocation when aa-tRNA was loaded in an eEF1A-dependent manner (Fig. 3D; SirDeshpande and Toogood 1995), which would be consistent with this model, since eEF2 and the ternary complex share binding sites on the ribosome (Marco et al. 2004). Indeed, this mode of action has been suggested for Did B previously and is the mechanism of action of the antibiotic kirromycin (Wolf et al. 1977; Ahuja et al. 2000; Andersen et al. 2003; Schmeing et al. 2009). It remains to be determined whether Cyt A binds directly to the ribosome and/or to eEF1A.

It has recently been suggested that tumor reduction caused by eIF4F inhibition may partially be caused by inhibiting angiogenesis (Graff et al. 2007; Cencic et al. 2009). Here, we show that Cyt A can also inhibit angiogenesis as Cyt A-inhibited HUVEC tube formation (Fig. 6A,B) as well as microvessel development in the CAM assay (Fig. 6D) in a manner similar to Did B (Taraboletti et al. 2004). These results suggest that Cyt A merits further study, not only for hematological cancers, but also for solid tumors requiring angiogenesis for optimal growth.

MATERIALS AND METHODS

Materials

Cyt A was prepared as previously described and stored in 100% DMSO (Kakeya et al. 1997). Didemnin B (Did B) (NCI-Developmental Therapeutics Program), homoharringtonine (HHT) (Sigma-Aldrich), and cycloheximide (CHX) (Bioshop) were stored in 100% DMSO, whereas anisomycin (Sigma) was resuspended in H_2O. Hippuristanol was purified as previously described (Bordeleau et al. 2006). All compounds were stored at −80°C.

Cell culture experiments

HeLa cells were grown in DMEM containing 10% fetal bovine serum and 100 U/mL penicillin/streptomycin. HUVEC cells (Lonza Walkersville, Inc.) were grown in EMB-2 medium supplemented with EGM-2.

For thymidine labeling of DNA, cells were serum starved for 48 h, followed by the addition of serum for 7 h, at which point

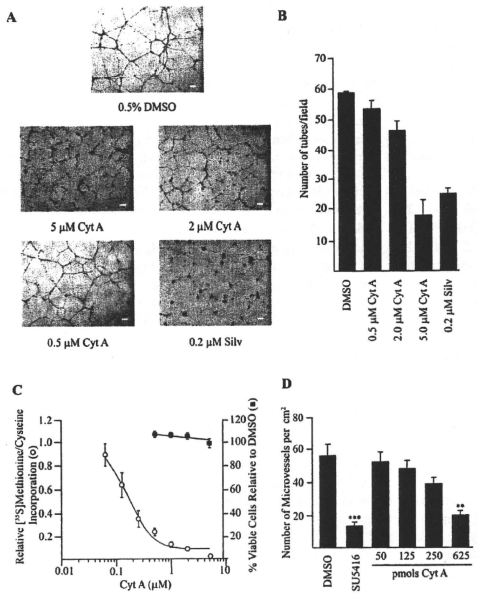

FIGURE 6. Cyt A inhibits angiogenesis. (*A*) Photomicrographs of HUVEC tube formation at different concentrations of Cyt A or silvestrol (Silv). Scale bar, 0.1 mm. (*B*) Quantitation of tube formation in HUVECs. Each well was photographed in seven fields, and the average number of tubes formed was counted. The average of four experiments is shown. Error bars represent the SEM. (*C*) Cyt A inhibits protein synthesis without inducing apoptosis in HUVECs. Following a 24-h exposure to Cyt A or DMSO, HUVECs were labeled for 20 min with [^{35}S]methionine/cysteine or monitored for apoptosis. For the translation assays, TCA-precipitable material was normalized to total protein content and set relative to the DMSO control. The average of four measurements is shown with the SEM represented by error bars. Cell viability was judged by the relative percent of Annexin-FITC or propidium iodide staining compared with DMSO controls. The average of five data points is shown with the SEM represented by error bars. (*D*) Cyt A inhibits angiogenesis in the CAM assay. Values presented represent the average number of vessels per cm^2 area for three samples with the SEM; $^{**}P < 0.01$ (vs. vehicle); $^{***}P < 0.001$ (vs. vehicle).

compound was added for 1 h. [6-^{3}H]thymidine (10 Ci/mmol) (Perkin Elmer) was present for the last 20 min of the reaction. For RNA labeling, cells were not serum starved and [5-^{3}H]uridine (26.3 Ci/mmol) (Perkin Elmer) was present during the last 20 min of a 1-h compound treatment. Cells were washed in PBS and lysed in RIPA buffer (50 mM Tris-HCl at pH 7.5, 150 mM NaCl, 1% NP-40, 0.5% sodium deoxycholate, 0.1% SDS). Radioactive incorporation was measured by TCA precipitation (5% TCA) onto GF/C filters (preblocked with 5% TCA and 0.1 M inorganic pyrophosphate). Filters were washed with 5 mL of cold 1% TCA, followed by 5 mL 100% ethanol, and quantified by scintillation counting. Counts were standardized to total protein content that had been determined using the D_c protein assay (Bio-Rad).

To monitor protein synthesis, cells were seeded into a 24-well dish and exposed to compound for 1 h with labeling performed during the last 20 min using [^{35}S]Easy Tag Express Protein Labeling mix (1175 Ci/mmol) (Perkin Elmer). Cells were lysed in RIPA buffer and an aliquot processed for TCA precipitation as described above.

HUVEC tube formation assays were performed as published previously (Cencic et al. 2009). HUVECs were seeded at 100,000 cell/well in the presence of compound on top of 300 μL of solidified BD Matrigel Matrix (BD Biosciences) in a 24-well dish. After 24 h, pictures were taken using a Nikon Eclipse TE300 microscope.

In vitro translation assays

In vitro translations were performed as previously reported (Novac et al. 2004). Translations were performed using a capped bicistronic mRNA reporter FF/HCV/Ren transcribed from pSP/$(CAG)_{33}$/FF/HCV/Ren.pA_{51}, in which firefly (FF) luciferase protein is produced by cap-dependent translation and *Renilla* (Ren) luciferase protein is generated by Hepatitis C virus (HCV) IRES-mediated initiation. Translation extracts were programmed with 8 μg/mL mRNA.

Experiments analyzing the consequences of Cyt A on actively translating ribosomes were performed in Krebs-2 extracts in the absence of in vitro-transcribed RNA, but in the presence of [^{35}S]methionine (Perkin Elmer), with compound being added 5 min after translation had been initiated. Aliquots (10 μL) were taken at the indicated times and added to 1.1 μL of 0.5 mM cycloheximide (CHX) and placed on dry ice to stop the reaction. Reactions were spotted onto 3 MM Whatman paper that had been preblocked with 50× amino acid mix (GIBCO). Filters were incubated in 10% TCA + 0.1% methionine on ice for 20 min, boiled in 5% TCA for 15 min, washed with 100% ethanol, dried, and the radioactivity quantitated by scintillation counting.

In vitro translation of poly(Phe) was performed in RRL using 50% RRL (Promega), 40 μM amino acid mix lacking phenylalanine, 40 μM methionine, 0.1 μg/μL poly(U) RNA, 4 μM magnesium acetate, 50 μM potassium acetate, and 50 μCi/mL [^{3}H]phenylalanine (Perkin Elmer). Following a 1-h incubation at 30°C, reactions were processed for TCA precipitation as described above.

Ribosome-binding assays and polysome profiling

Ribosome-binding assays were performed essentially as described previously (Robert et al. 2006). Briefly, compound was preincubated

with RRL at a final KCl concentration of 150 mM for 5 min, after which ^{32}P-labeled CAT mRNA was included. When a second compound was added, it was delivered 3 min after addition of RNA and reactions allowed to proceed at 30°C for 10 min. Reactions were centrifuged through a 10%–30% glycerol gradient at 39,000 rpm for 3.5 h in a SW40 rotor. Fractions (0.5 mL) were collected and quantitated by Cherenkov counting.

Polysome profiles of HeLa cells where visualized by treating cells with DMSO, 2 μM Cyt A, or 0.5 μM HHT for 1 h in a 10-cm^2 dish. Hippuristanol (5 μM) was added during the remaining 30 min. Cells were then washed in PBS containing 0.1 mg/mL CHX, scraped, and lysed in hypotonic lysis buffer (5 mM Tris-HCl at pH 7.5, 2.5 mM $MgCl_2$, 1.5 mM KCl, 0.1 mg/mL CHX, 2 mM DTT). The lysate was supplemented with 0.5% Triton X-100 and 0.5% sodium deoxycholate, centrifuged briefly (12,000*g* for 2 min), and the supernatant loaded onto 10%–50% sucrose gradients (20 mM HEPES-KOH at pH 7.5, 100 mM KCl, 5 mM $MgCl_2$, 1 mM DTT). Samples were centrifuged at 35,000 rpm for 2 h in a SW40 rotor at 4°C. The OD_{260} was monitored with a UA-6 UV detector (ISCO) using a Brandel tube piercer. Data was recorded using InstaCal Version 5.70 and TracerDaq Version 1.9.0.0 (Measurement Computing Corporation).

Peptidyl transferase assays

The peptidyl transferase assay was performed as previously described (Lorsch and Herschlag 1999). Briefly, [^{35}S]methionyl-$tRNA_i$ was generated by incubating 0.25 mg/mL total calf liver tRNA (Novogen) with 10 mM ATP, 10 mM CTP, 0.25 mg/mL leucovorin, 1 mCi/mL [^{35}S]methionine, and 0.875 μg/mL *E. coli* aminoacyl-tRNA synthetases (Sigma) in 50 mM sodium cacodylate (pH 7.4), 15 mM $MgCl_2$, and 7 mM 2-mercaptoethanol at 37°C for 30 min (Stanley 1974). Charged tRNA was purified by phenol/chloroform extraction, exclusion chromatography on a Sephadex G-50 spin-column, and ethanol precipitation.

Purified 40S and 60S ribosomes (0.06 μM) (Fraser et al. 2007), 0.5 mM GTP, 1 μM model RNA (GGAA[UC]$_7$UAUG[CU]$_{10}$C), 2 nM labeled [^{35}S]methionyl-$tRNA_i$, and a high-salt wash of ribosomes (Lorsch and Herschlag 1999) were incubated with 50 μM Cyt A. Reactions were subsequently started by the addition of 0.4 mM puromycin at 26°C. Aliquots were stopped in 0.4 M sodium acetate, spotted on cation-exchange IONEX-25 SA-Na TLC plates (Macherey-Nagel) (prerun in distilled water and dried), and developed in 2 M ammonium acetate and 10% acetonitrile. Experiments were visualized by phosphorimaging (Typhoon Trio, Amersham).

tRNA-binding and translocation assays

tRNA-binding and translocation assays were performed essentially as described (SirDeshpande and Toogood 1995; Robert et al. 2006). [^{14}C]Phe-$tRNA^{Phe}$ was prepared by charging 0.2 mg/mL yeast $tRNA^{Phe}$ (Sigma) with 3.75 mM ATP, 0.06 mM [^{14}C]phenylalanine in 50 mM Tris-HCl at pH 7.5, 20 mM $Mg(OAc)_2$, and 120 mM KCl using 10% (v/v) yeast S100 as the source of tRNA synthetase. Charged tRNA was purified via phenol/chloroform extraction, passed through a Sephadex G-50 spin-column, followed by ethanol precipitation (Odom et al. 1990).

For eEF1A-dependent assays, reactions were performed with 1.77 μM salt-washed 80S ribosomes, (0.4 μg/mL) poly(U) RNA, and 0.2 μM [^{14}C]Phe-$tRNA^{Phe}$ with 4.65 μg of eEF1A. Either 0.15 mM GMP-PMP, GDP, or GTP was added in HEPES buffer (20 mM HEPES at pH 7.5, 10 mM $MgCl_2$, 100 mM KCl, 1 mM DTT) and reactions (100 μL) were incubated at 37°C for 30 min. Aliquots (6% of the total reaction) were taken, diluted in 0.8 mL of HEPES buffer and filtered through Type HA nitrocellulose filters (Millipore). Amino acyl-tRNA binding was quantitated by scintillation counting and values obtained without ribosomes were subtracted to remove background. The remaining reaction volume (of samples containing GTP) was used to perform translocation assays. Additional GTP (1 mM) was added to 15% of the samples in the presence or absence of 0.5 mM puromycin and/or 0.05 μg/μL eEF2 and incubated at 37°C for 30 min. The reaction was quenched with 1 M NH_4HCO_3 and extracted with ethyl acetate. Ninety percent of the organic layer was used for quantitation by scintillation counting. A puromycin assay was performed on 10% of the original reaction to determine the amount of aminoacyl-tRNA already bound to the P-site (Wurmbach and Nierhaus 1979), which was normalized and deducted from the values obtained above to determine the total amount of tRNA translocated.

Nonenzymatic tRNA-binding reactions were performed essentially as described for eIF1A, except higher amounts of poly(U) RNA (0.4 mg/mL) were used, and the reaction was performed in the absence of both GTP (or its analogs) and eEF1A. Reactions were carried out in Tris reaction buffer (50 mM Tris-HCl at pH 7.5, 60 mM KCl, 20 mM $MgCl_2$) containing 50 μM of compound. Translocation assays were performed as described above, except that they were carried out in Tris reaction buffer.

eEF1A enzymatic assays

GTP cross-linking to eEF1A was performed in 20-μL reactions containing 1 μg of eEF1A and 2.5 μCi of [α-^{32}P]GTP (3000 Ci/mmol) (Perkin Elmer) with or without 0.8 μg of Phe-$tRNA^{Phe}$ (Sigma) in GTPase buffer (25 mM HEPES at pH 7.5, 125 mM KCl, 8.5 mM $MgCl_2$, 1 mM DTT). Reactions were incubated at 37°C for 15 min in the presence of 50 μM Cyt A, 1 mM cold GTP competitor, or DMSO, and cross-linked using a 254-nm germicidal UV lamp at 4°C for 15 min. Reactions were digested with 0.5 μg/μL RNase A for 10 min at 37°C, separated by SDS-PAGE, and visualized by autoradiography. Negative controls contained 1 μg of BSA instead of eEF1A.

Electrophoretic mobility shift assays were performed in 10-μL reactions in GTPase buffer using 0.5–2 μg of eEF1A and 1 mM GTP. Reactions were preincubated at room temperature for 10 min, after which time 20,000 cpm of [^{14}C]Phe-$tRNA^{Phe}$ was added, and the incubation continued for an additional 15 min. Equivalent molar amounts of unlabeled Phe-$tRNA^{Phe}$ were used as competitor. Reactions were analyzed on 6% native polyacrylamide (29:1 acrylamide:bisacrylamide) gels and electrophoresis performed in 1× TBE (90 mM Tris, 90 mM boric acid, 2 mM EDTA). Gels were then treated with En^{3}Hance (Perkin Elmer), washed in water, dried, and visualized by autoradiography.

GTPase assays (20 μL) were performed in GTPase buffer containing 0.5 μg of eEF1A and 1 μCi of [γ-^{32}P]GTP (6000 Ci/mmol) (Perkin Elmer) incubated with or without 0.8 μg of unlabeled Phe-$tRNA^{Phe}$, 16.8 pmol 40S, and 60S ribosomal subunits, and 31.4 pmol poly(U) RNA at 25°C. Control reactions were also performed without eEF1A or using only eEF1A (without tRNA, ribosomes or

RNA). Aliquots (2 µL) were taken and reactions stopped in 2 µL of 25 mM EDTA on ice. PEI Cellulose F TLC plates (EMD Chemicals, Inc.) were spotted with a 1.5-µL sample and developed using 0.3 M NaH_2PO_4/1 M $LiCl_2$. TLCs were quantitated using phosphorimaging on a Typhoon Trio (Amersham).

Viability assays

Viability assays were performed using Annexin-FITC and propidium iodide (PI) staining. HUVECs were treated with compound for 24 h in a 24-well plate. Cells were washed in PBS and trypsinized. Cells, PBS washes, and cell culture medium were collected together and centrifuged at 610*g* for 5 min. Cell pellets were washed in PBS and resuspended in 35 µL Annexin V binding buffer (10 mM HEPES-NaOH at pH 7.5, 140 mM NaCl, 2.5 mM $CaCl_2$). PI (Sigma) to a final concentration of 5 µg/mL and 1.75 µL FITC Annexin V (BD Biosciences Pharmingen) were added to reactions and incubated at RT for 20 min in the dark. Samples were diluted by the addition of 200 µL of Annexin V binding buffer and analyzed on a Guava Easy Cyte Plus (Millipore). Each experiment included unstained, PI-only, and Annexin V-only controls.

Chorioallantoic membrane (CAM) assay

The CAM assay was performed by Links Biosciences, LLC. Fertilized eggs were placed in an egg incubator at 37°C and 50% humidity. After 6 d, the egg shell was cracked and gently opened. A 5 × 5-mm sterile filter paper square saturated with either 25 µL of compound (50, 125, 250, 625 pmol), 4.2 nmol SU5416 (Sugen, Inc.), or vehicle (2% DMSO in PBS) was placed in areas between vessels. After 48 h, the CAMs were isolated and fixed in methanol/acetone. Representative images were collected by photography to permit quantitative analysis of vessel density.

ACKNOWLEDGMENTS

We thank Isabelle Harvey for technical assistance and Dr. T. Martin Schmeing for critical reading of the manuscript and insightful comments. L.L. was supported by a NSERC Alexander Graham Bell (CGSD) fellowship. This work was supported by a grant from the Canadian Cancer Society Research Institute (#20066) to J.P. and a NIH grant (R01 GM092927) to C.F.

Received June 7, 2010; accepted September 17, 2010.

REFERENCES

Ahuja D, Vera MD, SirDeshpande BV, Morimoto H, Williams PG, Joullie MM, Toogood PL. 2000. Inhibition of protein synthesis by didemnin B: How EF-1α mediates inhibition of translocation. *Biochemistry* **39:** 4339–4346.

Andersen GR, Nissen P, Nyborg J. 2003. Elongation factors in protein biosynthesis. *Trends Biochem Sci* **28:** 434–441.

Bordeleau ME, Mori A, Oberer M, Lindqvist L, Chard LS, Higa T, Belsham GJ, Wagner G, Tanaka J, Pelletier J. 2006. Functional characterization of IRESes by an inhibitor of the RNA helicase eIF4A. *Nat Chem Biol* **2:** 213–220.

Cencic R, Carrier M, Galicia-Vazquez G, Bordeleau ME, Sukarieh R, Bourdeau A, Brem B, Teodoro JG, Greger H, Tremblay ML, et al. 2009. Antitumor activity and mechanism of action of the cyclopenta[*b*]benzofuran, silvestrol. *PLoS ONE* **4:** e5223. doi: 10.1371/journal.pone.0005223.

Chan J, Khan SN, Harvey I, Merrick W, Pelletier J. 2004. Eukaryotic protein synthesis inhibitors identified by comparison of cytotoxicity profiles. *RNA* **10:** 528–543.

Chao JR, Wang JM, Lee SF, Peng HW, Lin YH, Chou CH, Li JC, Huang HM, Chou CK, Kuo ML, et al. 1998. mcl-1 is an immediate-early gene activated by the granulocyte-macrophage colony-stimulating factor (GM-CSF) signaling pathway and is one component of the GM-CSF viability response. *Mol Cell Biol* **18:** 4883–4898.

Crews CM, Collins JL, Lane WS, Snapper ML, Schreiber SL. 1994. GTP-dependent binding of the antiproliferative agent didemnin to elongation factor 1 alpha. *J Biol Chem* **269:** 15411–15414.

Duncan R, Milburn SC, Hershey JW. 1987. Regulated phosphorylation and low abundance of HeLa cell initiation factor eIF-4F suggest a role in translational control. Heat shock effects on eIF-4F. *J Biol Chem* **262:** 380–388.

Floss HG, Yu TW. 2005. Rifamycin-mode of action, resistance, and biosynthesis. *Chem Rev* **105:** 621–632.

Fraser CS, Berry KE, Hershey JW, Doudna JA. 2007. eIF3j is located in the decoding center of the human 40S ribosomal subunit. *Mol Cell* **26:** 811–819.

Graff JR, Konicek BW, Vincent TM, Lynch RL, Monteith D, Weir SN, Schwier P, Capen A, Goode RL, Dowless MS, et al. 2007. Therapeutic suppression of translation initiation factor eIF4E expression reduces tumor growth without toxicity. *J Clin Invest* **117:** 2638–2648.

Heffron SE, Jurnak F. 2000. Structure of an EF-Tu complex with a thiazolyl peptide antibiotic determined at 2.35 Å resolution: Atomic basis for GE2270A inhibition of EF-Tu. *Biochemistry* **39:** 37–45.

Heys SD, Park KG, McNurlan MA, Calder AG, Buchan V, Blessing K, Eremin O, Garlick PJ. 1991. Measurement of tumour protein synthesis in vivo in human colorectal and breast cancer and its variability in separate biopsies from the same tumour. *Clin Sci* **80:** 587–593.

Isaacs JS, Xu W, Neckers L. 2003. Heat shock protein 90 as a molecular target for cancer therapeutics. *Cancer Cell* **3:** 213–217.

Kahns S, Lund A, Kristensen P, Knudsen CR, Clark BF, Cavallius J, Merrick WC. 1998. The elongation factor 1 A-2 isoform from rabbit: Cloning of the cDNA and characterization of the protein. *Nucleic Acids Res* **26:** 1884–1890.

Kakeya H, Zhang HP, Kobinata K, Onose R, Onozawa C, Kudo T, Osada H. 1997. Cytotrienin A, a novel apoptosis inducer in human leukemia HL-60 cells. *J Antibiot* **50:** 370–372.

Kakeya H, Onose R, Osada H. 1998. Caspase-mediated activation of a 36-kDa myelin basic protein kinase during anticancer drug-induced apoptosis. *Cancer Res* **58:** 4888–4894.

Kubota Y, Kleinman HK, Martin GR, Lawley TJ. 1988. Role of laminin and basement membrane in the morphological differentiation of human endothelial cells into capillary-like structures. *J Cell Biol* **107:** 1589–1598.

Le Tourneau C, Raymond E, Faivre S. 2007. Aplidine: A paradigm of how to handle the activity and toxicity of a novel marine anticancer poison. *Curr Pharm Des* **13:** 3427–3439.

Lindqvist L, Pelletier J. 2009. Inhibitors of translation initiation as cancer therapeutics. *Future Med Chem* **1:** 1709–1722.

Lorsch JR, Herschlag D. 1999. Kinetic dissection of fundamental processes of eukaryotic translation initiation in vitro. *EMBO J* **18:** 6705–6717.

Lucas DM, Edwards RB, Lozanski G, West DA, Shin JD, Vargo MA, Davis ME, Rozewski DM, Johnson AJ, Su BN, et al. 2009. The novel plant-derived agent silvestrol has B-cell selective activity in chronic lymphocytic leukemia and acute lymphoblastic leukemia in vitro and in vivo. *Blood* **113:** 4656–4666.

Marco E, Martin-Santamaria S, Cuevas C, Gago F. 2004. Structural basis for the binding of didemnins to human elongation factor eEF1A and rationale for the potent antitumor activity of these marine natural products. *J Med Chem* **47:** 4439–4452.

Monks A, Scudiero D, Skehan P, Shoemaker R, Paull K, Vistica D, Hose C, Langley J, Cronise P, Vaigro-Wolff A, et al. 1991.

Feasibility of a high-flux anticancer drug screen using a diverse panel of cultured human tumor cell lines. *J Natl Cancer Inst* **83:** 757–766.

Nijhawan D, Fang M, Traer E, Zhong Q, Gao W, Du F, Wang X. 2003. Elimination of Mcl-1 is required for the initiation of apoptosis following ultraviolet irradiation. *Genes Dev* **17:** 1475–1486.

Novac O, Guenier AS, Pelletier J. 2004. Inhibitors of protein synthesis identified by a high throughput multiplexed translation screen. *Nucleic Acids Res* **32:** 902–915.

Odom OW, Picking WD, Hardesty B. 1990. Movement of tRNA but not the nascent peptide during peptide bond formation on ribosomes. *Biochemistry* **29:** 10734–10744.

Pelletier J, Peltz SW. 2007. Therapeutic Opportunities in Translation. In *Translational Control in Biology and Medicine*, (ed. MB Mathews et al.), pp. 855–895. Cold Spring Harbor Laboratory Press, Cold Spring Harbor, NY.

Quintas-Cardama A, Kantarjian H, Garcia-Manero G, O'Brien S, Faderl S, Estrov Z, Giles F, Murgo A, Ladie N, Verstovsek S, et al. 2007. Phase I/II study of subcutaneous homoharringtonine in patients with chronic myeloid leukemia who have failed prior therapy. *Cancer* **109:** 248–255.

Quintas-Cardama A, Kantarjian H, Cortes J. 2009. Homoharringtonine, omacetaxine mepesuccinate, and chronic myeloid leukemia circa 2009. *Cancer* **115:** 5382–5393.

Riboldi E, Musso T, Moroni E, Urbinati C, Bernasconi S, Rusnati M, Adorini L, Presta M, Sozzani S. 2005. Cutting edge: Proangiogenic properties of alternatively activated dendritic cells. *J Immunol* **175:** 2788–2792.

Robert F, Gao HQ, Donia M, Merrick WC, Hamann MT, Pelletier J. 2006. Chlorolissoclimides: New inhibitors of eukaryotic protein synthesis. *RNA* **12:** 717–725.

Robert F, Carrier M, Rawe S, Chen S, Lowe S, Pelletier J. 2009. Altering chemosensitivity by modulating translation elongation. *PLoS ONE* **4:** e5428. doi: 10.1371/journal.pone.0005428.

Rodnina MV, Wintermeyer W. 2001. Fidelity of aminoacyl-tRNA selection on the ribosome: Kinetic and structural mechanisms. *Annu Rev Biochem* **70:** 415–435.

Schmeing TM, Voorhees RM, Kelley AC, Gao YG, Murphy FV IV, Weir JR, Ramakrishnan V. 2009. The crystal structure of the ribosome bound to EF-Tu and aminoacyl-tRNA. *Science* **326:** 688–694.

Schneider-Poetsch T, Ju J, Eyler DE, Dang Y, Bhat S, Merrick WC, Green R, Shen B, Liu JO. 2010. Inhibition of eukaryotic translation elongation by cycloheximide and lactimidomycin. *Nat Chem Biol* **6:** 209–217.

SirDeshpande BV, Toogood PL. 1995. Mechanism of protein synthesis inhibition by didemnin B in vitro. *Biochemistry* **34:** 9177–9184.

Stanley WM Jr. 1974. Specific aminoacylation of the methionine-specific tRNA's of eukaryotes. *Methods Enzymol* **29:** 530–547.

Taraboletti G, Poli M, Dossi R, Manenti L, Borsotti P, Faircloth GT, Broggini M, D'Incalci M, Ribatti D, Giavazzi R. 2004. Antiangiogenic activity of aplidine, a new agent of marine origin. *Br J Cancer* **90:** 2418–2424.

Thornton S, Anand N, Purcell D, Lee J. 2003. Not just for housekeeping: Protein initiation and elongation factors in cell growth and tumorigenesis. *J Mol Med* **81:** 536–548.

Urdiales JL, Morata P, Nunez De Castro I, Sanchez-Jimenez F. 1996. Antiproliferative effect of dehydrodidemnin B (DDB), a depsipeptide isolated from Mediterranean tunicates. *Cancer Lett* **102:** 31–37.

Watabe M, Kakeya H, Onose R, Osada H. 2000. Activation of MST/Krs and c-Jun N-terminal kinases by different signaling pathways during cytotrienin A-induced apoptosis. *J Biol Chem* **275:** 8766–8771.

Wendel HG, De Stanchina E, Fridman JS, Malina A, Ray S, Kogan S, Cordon-Cardo C, Pelletier J, Lowe SW. 2004. Survival signalling by Akt and eIF4E in oncogenesis and cancer therapy. *Nature* **428:** 332–337.

Wolf H, Chinali G, Parmeggiani A. 1977. Mechanism of the inhibition of protein synthesis by kirromycin. Role of elongation factor Tu and ribosomes. *Eur J Biochem* **75:** 67–75.

Wurmbach P, Nierhaus KH. 1979. Codon-anticodon interaction at the ribosomal P (peptidyl-tRNA) site. *Proc Natl Acad Sci* **76:** 2143–2147.

nature chemical biology

ARTICLE

PUBLISHED ONLINE: 13 JUNE 2010 | DOI: 10.1038/NCHEMBIO.387

Marine antifungal theonellamides target 3β-hydroxysterol to activate Rho1 signaling

Shinichi Nishimura[1,2], Yuko Arita[3,4], Miyuki Honda[3,5], Kunihiko Iwamoto[6], Akihisa Matsuyama[3,7], Atsuko Shirai[3], Hisashi Kawasaki[5], Hideaki Kakeya[1,2], Toshihide Kobayashi[6], Shigeki Matsunaga[8] & Minoru Yoshida[1,3,4,7]*

Linking bioactive compounds to their cellular targets is a central challenge in chemical biology. Here we report the mode of action of theonellamides, bicyclic peptides derived from marine sponges. We generated a chemical-genomic profile of theonellamide F using a collection of fission yeast strains in which each open reading frame (ORF) is expressed under the control of an inducible promoter. Clustering analysis of the Gene Ontology (GO) terms associated with the genes that alter drug sensitivity suggested a mechanistic link between theonellamide and 1,3-β-D-glucan synthesis. Indeed, theonellamide F induced overproduction of 1,3-β-D-glucan in a Rho1-dependent manner. Subcellular localization and *in vitro* binding assays using a fluorescent theonellamide derivative revealed that theonellamides specifically bind to 3β-hydroxysterols, including ergosterol, and cause membrane damage. The biological activity of theonellamides was alleviated in mutants defective in ergosterol biosynthesis. Theonellamides thus represent a new class of sterol-binding molecules that induce membrane damage and activate Rho1-mediated 1,3-β-D-glucan synthesis.

Cyclic and branched cyclic peptides are a large family of natural products with a rich diversity of both structure and activity. They often contain unusual amino acids in the peptide backbone and sometimes possess characteristic modifications in the side chains. Cyclic peptides show a broad range of biological activities including antibacterial, antifungal, immunosuppressive and anticancer activities. Daptomycin, for example, binds bacterial cell membrane and is used as an antibiotic to treat infections caused by Gram-positive bacteria[1]. Antifungal echinocandins including caspofungin and micafungin (FK463) impair cell wall synthesis by inhibiting 1,3-β-D-glucan synthase[2]. Cyclosporin A, which inhibits calcineurin after binding its cellular targets cyclophilins, possesses immunosuppressive activity and is used clinically in organ transplantation[3]. In addition, echinomycin[4,5] and didemnin B[6], which bind DNA and the EF-1α–ribosome complex, exert anticancer activity by inhibiting hypoxia-inducible factor-1 binding to DNA and inhibiting protein synthesis, respectively. Most of these cyclic peptides are synthesized by nonribosomal peptide synthetases, which are widespread among microorganisms. Marine sponges are also an abundant source of this class of bioactive peptides[7].

Theonellamides (TNMs) are members of a unique family of bicyclic dodecapeptides isolated from a marine sponge, *Theonella* sp. These compounds show broad antifungal activity as well as moderate cytotoxicity to mammalian cells[8,9]. Theonegramide[10], theopalauamide and isotheopalauamide[11] are related compounds with minor modifications at specific amino acid side chains. These compounds have a characteristic bicyclic structure bridged by a histidinoalanine residue. A subfamily of compounds contains a sugar group on the imidazole ring at the center of the molecule. The reported biological activities of these compounds were comparable regardless of the presence of the sugar group, suggesting that the characteristic bicyclic peptide framework is responsible for their specific biological actions. Despite screens for binding proteins using TNM-A (**1**) affinity beads[12], their target molecules—that is, those that bind directly to TNMs—remain unknown.

In this study, we screened for genes that confer altered sensitivity to TNM-F (**2**, **Fig. 1a**) in fission yeast cells to gain insight into the mode of action of TNMs. Our screen design took advantage of the fission yeast ORFeome overexpression strain collections[13,14]. Comparison of the chemical-genomic profiles, functional analyses of products of the identified genes and binding assays using a fluorescently labeled theonellamide derivative revealed that TNM-F is a sterol-binding molecule that causes membrane damage and increases cell wall synthesis in a Rho1-dependent manner.

RESULTS

Characterization of TNM-F by chemical-genomic profiling

Screens for binding proteins have already been carried out using TNM-A affinity beads[12]. Thus far, none of the proteins identified appear to be the target responsible for the cytotoxicity. Our group also made TNM affinity beads by a photo-affinity immobilization method[15] and tried to identify the binding proteins from fission yeast cells, but we could not detect any proteins specifically bound to TNM-F (**Supplementary Fig. 1**). We therefore decided to search for chemical-genetic interactions using a set of strains expressing all ~5,000 protein-coding ORFs—the 'ORFeome'—of the fission yeast *Schizosaccharomyces pombe*[13,14], which might provide insights into the genes and pathways targeted by bioactive metabolites. In this collection, each ORF is inserted into the chromosomal *leu1* locus and is expressed as a C-terminally fused protein with two Flag epitopes and one hexahistidine tag under the control of the *nmt1* inducible promoter, which generally leads

[1]Chemical Genomics Research Group, RIKEN Advanced Science Institute, Saitama, Japan. [2]Division of Bioinformatics and Chemical Genomics, Graduate School of Pharmaceutical Sciences, Kyoto University, Kyoto, Japan. [3]Chemical Genetics Laboratory, RIKEN Advanced Science Institute, Saitama, Japan. [4]Graduate School of Science and Engineering, Saitama University, Saitama, Japan. [5]Department of Green and Sustainable Chemistry, Tokyo Denki University, Tokyo, Japan. [6]Lipid Biology Laboratory, RIKEN Advanced Science Institute, Saitama, Japan. [7]CREST Research Project, Japan Science and Technology Corporation, Saitama, Japan. [8]Graduate School of Agricultural and Life Sciences, The University of Tokyo, Tokyo, Japan. *e-mail: yoshidam@riken.jp

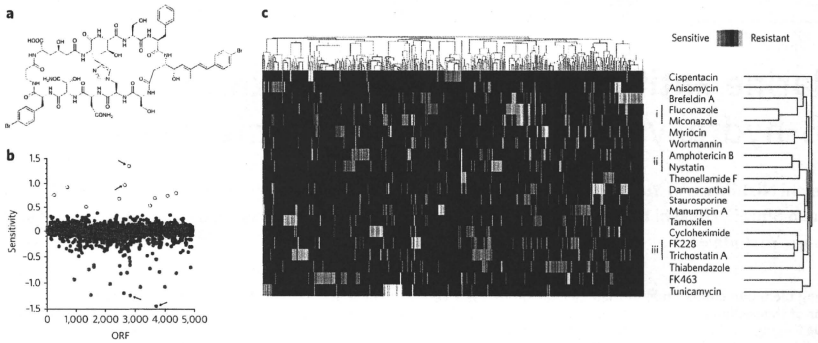

Figure 1 | Generation of chemical-genomic profiles. (**a**) Chemical structure of TNM-F. (**b**) Chemical-genomic profile of TNM-F. Ten ORFs conferring resistance (yellow) and 22 conferring hypersensitivity (blue) were identified (see **Supplementary Table 2** for detail). The *y* axis indicates the $\log_2$ of normalized AUC values, which were obtained from the growth curve of the corresponding transformant in the presence of various concentrations of TNM-F. Arrows indicate representative interactions: *SPCC23B6.04c* and *SPBC23G7.06c* are the top two resistance-conferring ORFs, whereas *SPAC26A3.09* (also known as *rga2*) and *SPAC17G8.14c* (also known as *pck1*) are the top two ORFs conferring hypersensitivity (see **Supplementary Fig. 2**). (**c**) Two-dimensional hierarchical clustering analysis of the 20 compound profiles. Compounds showing similar chemical-genomic profiles were clustered on the vertical axis; 575 ORFs are plotted on the horizontal axis on the basis the degree of hypersensitivity (blue) and resistance (yellow). Compounds possessing same target molecules are labeled with Roman numerals.

to overexpression of the gene product (**Supplementary Fig. 2**). Only a small subset, consisting of 169 strains that showed severe growth retardation upon overexpression, was excluded from our analysis (**Supplementary Data Set 1**). The overexpression strains were exposed individually to TNM-F and a compendium of ten reference compounds with known targets at various concentrations (**Supplementary Fig. 2** and **Supplementary Table 1**). Cell viability in liquid culture was measured using a colorimetric assay (XTT kit) and ranked quantitatively (**Supplementary Data Set 2**). Strains showing a significantly altered sensitivity compared to the control strain were selected and tested two more times. ORFs corresponding to the strains that were positive in all three rounds of screens were subjected to functional analysis (**Fig. 1b**, **Supplementary Data Set 3**).

We analyzed the chemical-genomic profiles by two-dimensional hierarchical clustering analysis[16] and compared the results with those obtained with TNM-F. The dendrogram suggested that these 11 compounds each function via distinct mechanisms (data not shown). To increase the profiles of target-known compounds, we selected approximately 600 strains that showed significant interactions with at least one of the 11 compounds and generated chemical-genetic profiles of nine other compounds using the selected strains (**Supplementary Table 1** and **Supplementary Data Set 4**). Thus, a total of 20 profiles were obtained, which we analyzed by two-dimensional hierarchical clustering analysis (**Fig. 1c**, **Supplementary Fig. 3** and **Supplementary Data Set 5**). We found a weak correlation with polyene antifungals amphotericin B (AMB) and nystatin (correlation coefficient = 0.18), implying that the mode of action of TNM-F is partially shared with these sterol binders.

In addition to pattern-matching analysis, information about the function of genes that alter sensitivity to the query compound (in other words, the hit genes) should be useful in predicting the target or its pathway. In the case of TNM-F, the gene conferring the strongest resistance was *SPCC23B6.04c*, which is predicted to encode a Sec14 homolog (**Supplementary Table 2**). The most sensitive strain overexpressed *SPAC26A3.09*, which encodes a homolog of Rho-type GTPase activating protein Rga2. The second most sensitive overexpressed *pck1*, which encodes a protein kinase C homolog that regulates 1,3-β-D-glucan synthesis[17].

We next determined GO terms with statistically significant enrichment ($P < 0.02$) in the hit genes for the initially tested 11 compounds and ranked them on the basis their extent of enrichment (**Supplementary Data Set 6**). This analysis showed that the hit genes for TNM-F were most enriched for GO terms related to cell polarity and signal transduction. However, none of these hit gene products appeared to be the primary target of TNM, because no physical interaction with immobilized TNM was detected (**Supplementary Fig. 1**). Furthermore, we carried out two-dimensional hierarchical clustering analysis of the enriched GO terms to compare with target-known compounds and found a modest linkage (correlation coefficient = 0.35) between TNM-F and FK463, a frontline clinical antifungal drug that inhibits the synthesis of 1,3-β-D-glucan[18] (**Supplementary Fig. 4**).

Counteraction of TNM-F with FK463

Of 32 TNM-F hit genes, 12 genes were in common with FK463, suggesting that modes of action of TNM-F and FK463 are functionally related (**Fig. 2a**). In contrast, TNM-F shared only two hit genes with nystatin. To see whether TNM-F also affects 1,3-β-D-glucan synthesis, we compared morphology of the cells after drug exposure. FK463 induced cell lysis at the growing ends in fungi by disrupting cell wall integrity (**Fig. 2b**), whereas TNM-F cells did not show any signs of cell lysis (**Fig. 2c,d**). Unexpectedly, however, calcofluor white (Cfw) staining showed strong signals at the growing ends and/or the medial region of the cells treated with TNM-F (**Fig. 2c,d**). Because TNM-F failed to increase the fluorescence in the *bgs1* mutant[19], in which the activity of the encoded 1,3-β-D-glucan synthase is greatly reduced (**Fig. 2e,f**), we suspected that the strong Cfw staining was due to increased 1,3-β-D-glucan synthesis. Similar images were also obtained using another fluorescent dye, aniline blue, which binds specifically to 1,3-β-D-glucans (**Supplementary Fig. 5**)[20]. AMB and nystatin did not increase the Cfw signal (**Fig. 2g**). Notably, the addition of TNM-F following FK463 treatment rescued the cells from FK463-induced cell lysis (**Fig. 2h**). Thus, TNM-F appears to

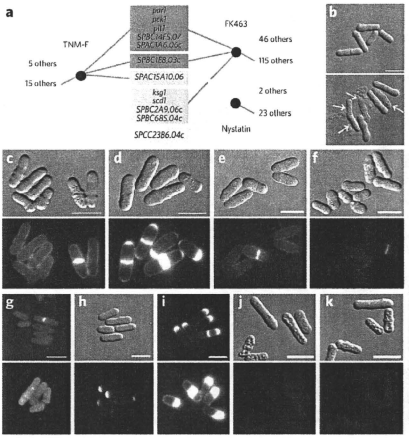

Figure 2 | Cell wall abnormality predicted by GO term analysis. (**a**) Chemical genetic interactions between TNM-F and FK463 or nystatin. Genes whose overexpression conferred resistance are shown in yellow, whereas those whose overexpression conferred hypersensitivity are shown in blue. Green boxes represent genes having opposite effects on TNM-F and FK463. (**b**) Cell lysis caused by FK463. Wild-type cells were treated with (lower) or without (upper) FK463 (20 μg ml^{-1}) for 2.5 h in the presence of 1.2 M sorbitol. FK463-treated cells showed the lysis phenotype (arrows). (**c**,**d**) Abnormal cell wall morphology induced by TNM-F. Yeast cells (HM123) were exposed to DMSO (**c**, 0.5% (v/v), solvent for TNM-F) or TNM-F (**d**, 5 μg ml^{-1}) for 2 h. (**e**,**f**) Bgs1 is required for aberrant Cfw staining by TNM-F. The strong Cfw signals were not observed in *bgs1* temperature-sensitive mutant cells incubated with DMSO (**e**, 0.5% (v/v)) or TNM-F (**f**, 5 μg ml^{-1}) at 27 °C for 2 h. (**g**) Effect of polyene antifungals on cell wall synthesis. Wild-type cells were treated with AMB (0.25 μg ml^{-1}, upper) or nystatin (1.6 μg ml^{-1}, lower) for 3 h. (**h**) Counteraction of FK463-induced cell lysis by TNM-F. (**i**–**k**) Involvement of Rho1 in the TNM-F–induced cell wall abnormality. Cells transformed with empty vector (**i**, upper), pREP41-Rho1 (**i**, lower) or pREP81-Rho1T20N (**j**,**k**) were grown at 30 °C for 15 h in MM liquid medium and then challenged with TNM-F (**i**,**k**) or DMSO (**j**) for an additional 2 h. Scale bars, 10 μm. In **c**–**k**, compound-treated cells were fixed and stained with Cfw. In **c**–**f**, **h**, **j** and **k**, differential interference contrast (DIC; upper) and Cfw (lower) images are shown.

counteract FK463 action by enhancing 1,3-β-D-glucan synthesis. Indeed, five genes identified as the hit genes of TNM-F and FK463 oppositely altered sensitivity to these compounds (**Fig. 2a**).

Rho1 mediates TNM-F–induced morphological abnormalities

1,3-β-D-Glucan is synthesized by transmembrane catalytic subunits in the presence of a regulatory subunit, a prenylated Rho1 (ref. 21). Rho1 is a small GTPase that plays a pivotal role in the signaling pathway involved in the regulation of cell polarity and in 1,3-β-D-glucan synthesis in fission yeast[21–23]. To test whether the TNM-induced 1,3-β-D-glucan synthesis is mediated by the activated Rho1 protein, we expressed a wild-type Rho1 in some cells and a dominant-negative Rho1 (Rho1T20N)[23] in others, using an inducible promoter. The overexpression of wild-type Rho1 greatly enhanced the Cfw staining induced by TNM-F (**Fig. 2i**). On the other hand, overexpression of Rho1T20N clearly inhibited the TNM-induced 1,3-β-D-glucan synthesis (**Fig. 2j**,**k**). Thus, the action of TNM-F appears to require Rho1. Rho1's effects are mediated by its interaction with at least three targets: 1,3-β-D-glucan synthase[21] and the protein kinases Pck1 and Pck2 (ref. 17,24), all of which are involved in 1,3-β-D-glucan synthesis. Deletion of neither *pck1* nor *pck2* abolished the increased Cfw staining induced by TNM-F (**Supplementary Fig. 6**). These results suggest that the major pathway to 1,3-β-D-glucan synthesis upon TNM-F treatment is the direct activation of Bgs1 by Rho1. However, Rho1T20N did not suppress the binding and cytotoxicity of TNM (**Supplementary Figs. 7** and **8**), suggesting that aberrant 1,3-β-D-glucan synthesis is not the primary reason for the TNM's cytotoxicity.

TNMs bind to 3β-hydroxysterols

To determine the subcellular localization of the TNM-binding molecule, we synthesized a fluorescently labeled TNM derivative (**3**, **4**, TNM-BF) by conjugating a 4,4-difluoro-5,7-dimethyl-4-bora-3a,4a-diaza-*s*-indacene-3-propionic acid moiety (BODIPY-FL) to the β-D-galactose moiety of TNM-A (**Supplementary Fig. 9**). TNM-BF was as active as TNM-F in inhibiting cell growth of wild-type *S. pombe* (**Supplementary Fig. 10**). Fluorescence microscopy clearly showed that TNM-BF is distributed at cell tips and in the septation region of cells undergoing cytokinesis (**Fig. 3a**). According to our Localizome dataset (available here: http://www.riken.jp/SPD/index.html), which assigned each of the 4,429 proteins to one of 17 possible subcellular localizations[13], approximately 80 proteins showed similar localization to TNM-BF (**Supplementary Data Set 7**). GO analysis revealed that transmembrane transporters were significantly enriched among these proteins (**Supplementary Table 3**). Transporters and lipid molecules have a close functional relationship (for example, Pma1 (**Fig. 3b**) is a marker for the lipid raft[25], a characteristic membrane microdomain rich in ergosterol and sphingolipids[26]). The proper localization of Pma1 depends on ergosterol biosynthesis[27]. On the basis of these observations, we theorized that the target of TNM could be a lipid molecule distributed in a polarized manner, rather than a protein. A binding assay using plasma membrane lipid components revealed that TNM-BF selectively recognizes ergosterol but not other lipids tested (**Fig. 3c**). In addition to ergosterol, TNM-BF bound to cholesterol, cholestanol and 5α-cholest-7-en-3β-ol (**Fig. 3d**,**e**). In contrast, a ketone group, an α-hydroxyl group or an esterification of the hydroxyl group at C3 position abolished the binding, indicating that TNM recognizes 3β-hydroxysterols (**Fig. 3e**).

Filipin, a fluorescent compound that forms a specific complex with 3β-hydroxysterols in the cell membrane[28], stained the cell periphery and medial region of cells undergoing cytokinesis[29] in a pattern very similar to that of TNM-BF, suggesting that the target of TNM-F in wild-type *S. pombe* is ergosterol, the major sterol in fungi. Double staining showed a clear overlap of the signals for the two compounds, but the region stained with TNM-BF was slightly more confined (**Fig. 3f**).

In vivo ergosterol distribution is regulated in a cell cycle–dependent manner in fission yeast[29], probably as a result of some function of actin[25,30]. Indeed, we also observed that latrunculin A treatment disrupted the polarity of filipin staining (**Supplementary Fig. 11**). Notably, latrunculin A reduced the fluorescent signal of TNM-BF to an almost undetectable level. Similarly, in a strain possessing an *act1* (also known as *cps8*) temperature-sensitive allele[30,31] both filipin and TNM-BF stained the cell tips and around the septum, as observed in wild-type cells at the permissive temperature, but their polarized localization was lost after temperature shift (**Supplementary Fig. 11**). It should be noted that the decrease in TNM-BF fluorescence was again observed in the *act1* mutant cells at 30 °C. It seems possible that proper organization of the sterol-rich membrane domain is required for TNM binding of the cell membrane. Indeed, overexpression of hit genes *scd1* and *rga2*, both

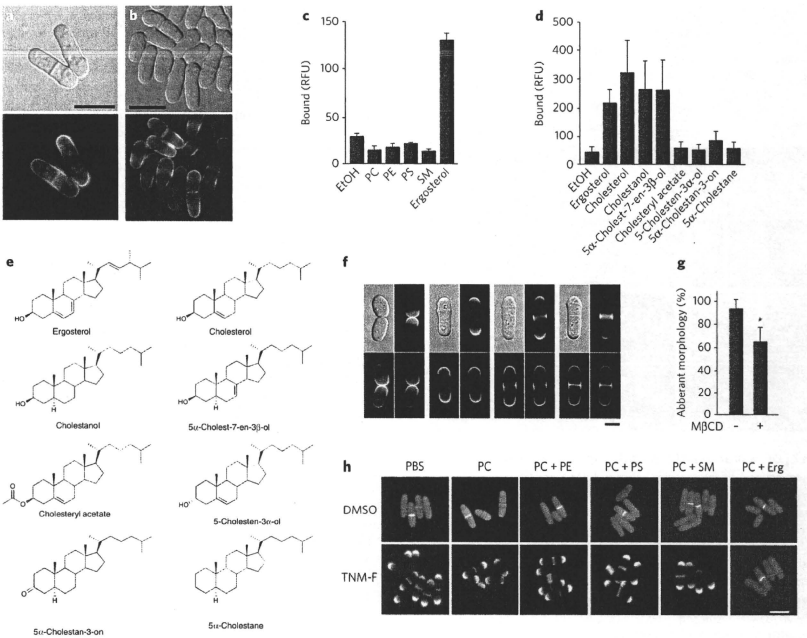

Figure 3 | Identification of 3β-hydroxysterols as the target of TNM-F. (**a**) The fluorescent image of cells stained by TNM-BF. (**b**) An example of protein localization similar to TNM-BF localization. The fluorescent image of the YFP-fused Pma1 is shown. (**c**) Binding of TNM-BF to ergosterol *in vitro*. (**d**) Binding of TNM-BF to various sterols *in vitro*. (**e**) Structure-affinity relationships of sterols. Functionalities colored in blue are not necessary for recognition by TNM-BF, whereas the red-colored structures hamper binding to TNM-BF. (**f**) Co-localization of TNM-BF with filipin. TNM-BF (upper right panels and red in merged images) and filipin (lower left panels and green in merged images) signals were observed in the similar region. Images of cells at different cell cycle stages are shown. (**g**) Effects of ergosterol extraction on the TNM-F–induced cell wall abnormality. Cells were preincubated in the presence (+) or absence (−) of methyl-β-cyclodextrin (MβCD) and then treated with TNM-F. After Cfw staining, cells with abnormally strong signals were counted. Asterisk indicates statistically significant difference ($P < 0.02$). See **Supplementary Figure 13** for details. (**h**) Effects of ergosterol-containing vesicles on TNM-F–induced cell wall abnormalities. Cells were treated with TNM-F (5 μg ml^{-1}) that had been preincubated with POPC vesicles or POPC-based vesicles containing PE (PC + PE), PS (PC + PS), SM (PC + SM) or ergosterol (PC + Erg) for 30 min. After 3 h incubation with TNM-F, cells were fixed and stained with Cfw. Scale bars are 10 μm except that in **f**, which is 5 μm. Data represent means of three (**c**,**d**) or four (**g**, $n > 110$ for each experiment) independent experiments. In **c**,**d** and **g**, error bars indicate s.d. RFU: Relative fluorescence units.

of which are involved in regulation of the actin cytoskeleton[32–34], caused a drastic decrease and increase, respectively, in TNM-BF staining (**Supplementary Fig. 12**).

Sterol binding is required for action of TNM-F

We next determined whether 3β-hydroxysterols are also required for TNM-induced 1,3-β-D-glucan synthesis. First, pretreatment of cells with methyl-β-cyclodextrin, which could extract a substantial amount of ergosterol (**Supplementary Fig. 13**), significantly reduced the number of cells showing an enhanced Cfw signal (**Fig. 3g**). Second, preincubation of TNM-F with 1-palmitoyl-2-oleoyl-*sn*-glycero-3-phosphocholine (POPC)-based multilamellar vesicles did not affect TNM-enhanced Cfw staining, but preincubation with vesicles containing ergosterol abolished it (**Fig. 3h**). These results suggest that pre-absorption of TNM-F with the ergosterol-rich membrane alleviates the action of TNM-F. Furthermore, latrunculin A treatment, which inhibits TNM-BF binding of cells, also hampered the TNM-F–induced abnormal Cfw staining (**Supplementary Fig. 14**). Thus, we conclude that a structured membrane domain rich in ergosterol and related sterols is required for the binding of TNM-F to exert its effects on the cell wall.

Effects of *erg* mutations on TNM-F sensitivity

Genetic mutations in the ergosterol biosynthetic pathway (**Fig. 4a**) have been shown to modulate sensitivity to polyene antibiotics in yeast[27,35]. In *S. pombe erg* mutants, ergosterol production is not detectable; however, filipin staining is not abolished, implying that sterols with filipin-binding activity other than ergosterol can still be produced and that they compensate for the roles of ergosterol[27]. Lack of Erg2, the putative enzyme that converts fecosterol to episterol, or simultaneous deletion of two *erg3*$^+$ homologs, *erg31* and *erg32*, both of which encode putative enzymes catalyzing the